國立臺灣大學理學院大氣科學系
碩士論文
Department of Atmospheric Science
College Science
National Taiwan University
Master Thesis

平衡渦旋模型之熱與動量動力效率
Dynamic Efficiency of Heat and Momentum in Balanced Vortex Model

許天耀
Tien-Yiao Hsu

指導教授：郭鴻基博士
Advisor: Hung-Chi Kuo, Ph.D.

中華民國 104 年 7 月
July, 2015

誌謝

一篇作品的完成不只需要個人努力，亦需有旅途中各方貴人的相助。

感謝郭老師給予的指導，討論，支持與肯定。這是我前進的動力。美雲超過兩年的關懷與照顧，無法用三言兩語表達，除了感謝還是感謝。維毅，虹叡，郁涵，徐驊，世顥，佑宇，政友，王珩，立中，佳瑩，映如等人給予的協助點滴在心。這是一間溫暖且包容的實驗室，有緣於此停泊，甚感幸運。緣分的推演人無可知，而我感謝這些安排。我要感謝家人與韋龍，在這些日子裏承擔我的任性。

最後，我要感謝自己，完成當初的承諾。這些日子裡，你更認識了自己，接受自己的缺點，也知道自己可以成為甚麼樣的人——你比過去更有能力參與自己的人生，謝謝你。

寫下這些文字的同時，窗外蟬聲唧唧，正如同兩年前的今天一樣，瀰漫著慵懶與未知。不同的是我即將完成學業離開此處。走入未來，如同走入森林，失去方向，充滿恐怖與不安，卻帶點雀躍和悸動。何處存在美麗的瀑布與甘泉？尋得之時必然知曉，因吾等已然品嘗。

2015/06/25 天耀

於一片唧唧蟬聲

摘要

觀測資料顯示眼牆置換 (ERC) 過程會產生不同的結果。Kuo et al. (2009) 發現在置換過程結束後，大約 28% 的颱風會繼續增強。Yang et al. (2013) 針對雙眼牆置換完成後的演化，發展出四個分類。他們指出不同分類的颱風在強度的演化上有明顯的不同，於 T-V 圖中亦具有不同的演化路徑。

Hack and Schubert (1986) 提出熱動力效率 $\eta(r,z,t)$ 之概念。此物理量能夠定量描述總位能 (**P**) 轉換到總動能 (**P**) 之能量轉換速率 (**C**)，並以加熱 (Q) 最為量度基準。該文獻指出儘管總加熱量 (**H**) 維持一樣，不同的渦漩結構會產生極為不同的轉換效率。在此研究中，我們將利用熱動力效率，來測試單雙眼牆颱風 Francis (2004) 之轉換效率反應。我們發現外眼牆在動力上能夠透過減少羅士比長度而提高渦漩的能量轉換效率達 50% 至 400%，而改變內外眼牆之加熱率比重 (從 1 : 2 至 2 : 1) 則可以強化能量轉換效率達 100% 至 600%。

除了此研究主要使用的圓柱座標外，本論文也推導在準地轉理論 (卡式座標)，卡式座標，球座標與淺水模型之動力效率，可供參考與應用於其他尺度平衡動力研究之用。

關鍵字：平衡渦漩、熱動力效率、動量動力效率、雙眼牆、次環流

ABSTRACT

The observation data shows that the eyewall replacement cycle (ERC) results in different consequences. Kuo et al. (2009) found that approximately 28% of typhoons strengthen after the formation of secondary eyewall. Yang et al. (2013) developed four categories to classify the situations after the formation. They found these four categories exhibit different behaviors on intensity and routes on T-V diagram.

"Dynamic efficiency of heat" $\eta\left(r,z,t\right))$ developed by Hack and Schubert (1986) is to examine the effect of heating on the energy conversion rate (**C**) converting total potential energy (**P**) into total kinetic energy (**K**) They also pointed out that efficiencies vary under different vortex structures while total heating remains the same. In this study, we would apply dynamic efficiencies to examine the response of concentric eyewall cyclone Francis (2004). We find that the presence of outer eyewall enhances the efficiency response by approximately 50% to 400% through reducing Rossby length (λ_R) while changing the heating ratio between inner and outer eyewalls from $1:2$ to $2:1$ enhances the efficiency by 100% to 600% (total heating is fixed).

Apart from cylindrical coordinates, we also derive the dynamic efficiencies in quasi-geostrophic theory (Cartesian coordinates), Cartesian coordinates, spherical coordinates, and shallow water model for potentially application to other balance dynamics in different scales.

Keywords: balanced vortex, dynamic efficiency of heat, dynamic efficiency of momentum, concentric eyewall, double eyewall, secondary circulation

CONTENTS

LIST OF FIGURES

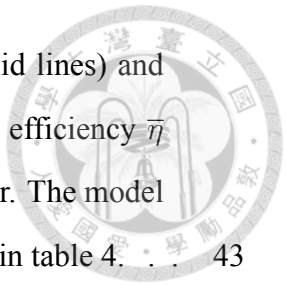

LIST OF TABLES

CHAPTER 1
INTRODUCTION

A cyclone intensifies itself by storing the available potential energy through latent of water vapor and releasing it into kinetic energy. Charney and Eliassen (1964) proposed Condition Instability of the Second Kind (CISK) to explain the initiation of the tropical depression. Later, Schubert and Hack (1982) demonstrated that pre-existing vortex is another important factor for constructing a warm core for it reduces Rossby deformation length (λ_R). It is also known that given the same amount of energy input, not necessarily every cyclone grows. By observation data, the eyewall replacement cycle after the generation of outer eyewall (some hypothesis were given by Rozoff et al., 2008) have different consequences (Kuo et al., 2009; Yang et al., 2013). The work above suggest the need of finding a way to quantify the effect of structure of heating and wind profile on kinetic energy of a cyclone.

Assuming an air column is heated uniformly by 10K per day (equivalent to the latent heat produced by 40mm per day) and its mass is 10^4 kg per 1 m^2. Energy released in 1 m^2 is

$$\Delta T \cdot c_p \cdot \text{Mass} = 10\,\text{K} \cdot 1004\,\text{J}\,\text{kg}^{-1}\,\text{K}^{-1} \cdot 10^4\,\text{kg} \approx 10^8\,\text{J}. \tag{1.1}$$

If 1% of heating energy can be converted into kinetic energy, then we have

$$10^8\text{J} \cdot 1\% = \frac{1}{2} \cdot 10^4\,\text{kg} \cdot \left(v_{\text{final}} - v_{\text{initial}}\right)^2, \tag{1.2}$$

where v_{initial} and v_{final} represent the initial and final velocities of the air column.

Let $v_{\text{initla}} = 0$, then we obtain

$$v_{\text{final}} = 10\sqrt{2}\,\text{m}\,\text{s}^{-1} \approx 14\,\text{m}\,\text{s}^{-1}. \tag{1.3}$$

Since wind speed over $17\text{m}\,\text{s}^{-1}$ will be identified with tropical storm in Saffir–Simpson hurricane wind scale, heating efficiency about 1% is significant enough in our studies.

To quantify the effect of heating, Hack and Schubert (1986) developed the idea of dynamic efficiency $\eta\,(r, z)$ to describe the efficiency of heating at particular position with the aid of Eliassen-Sawyer circulation equation. This tool is especially convenient for it requires only temperature profile $\theta\,(r, z)$ so that we can discuss without considering too much issue about adiabatic heating Q.

Contents in later chapters are structured as follows: Eliassen-Sawyer circulation equation and dynamic efficiency of heat and momentum will be derived in chapter 2. Relaxation method used in this paper in order to solve Eliassen-Sawyer circulation equation will be introduced in chapter 3. In chapter 4 will introduce our diagnose procedure, experiment settings and results. Summary is in chapter 5.

CHAPTER 2
FORMULATION

We will derive dynamic efficiencies in five different realms. Sec. 2.1 is the derivation in quasi-geostrophic theory of Cartesian coordinates, which serves as an friendly opening to readers unfamiliar with this topic since this theory is well-known to most of the meteorologists. Sec. 2.2 is the derivation in Cartesian coordinates without scaling like quasi-geostrophic theory. Sec. 2.3 is the derivation in cylindrical coordinates, which we apply to analyze tropical cyclone in particular. Sec. 2.4 is the derivation in spherical coordinates, showing that dynamic efficiencies can also work in planetary scale. In the end, the intrinsic shared properties of derivation above can be seen in the shallow water model of cylindrical coordinates, where we will also derive dynamic efficiencies for it, too.

Readers might note that the governing equations in Secs. 2.2-2.5 have no turbulent fluxes. In fact, turbulent fluxes can be included in external forcings (diabatic heating and momentum source), so dynamic efficiencies are essentially symmetry dynamics. As a result, it is better to keep turbulent fluxes away to avoid confusion in these sections. We keep, however, turbulent fluxes in Sec. 2.1 to retain connections to other studies because turbulent fluxes are essential to quasi-geostrophic in most applications.

In our basic framework, the system is closed, i.e., no air can go across the boundaries. App. C discusses the situations when bottom boundary is connected to the planetary boundary layer and is not closed.

Of theory interest, inertial buoyancy waves can also be combined with Eliassen-Sawyer circulation equation to get a clearer understanding of balanced systems. It can be shown that the product of maximum and minimum frequencies of inertial buoyancy wave is a constant which is related to the Jacobian determinant of absolute angular momentum

and buoyancy force. These discussions are presented in App. B.

2.1 Efficiency in Quasi-geostrophic Theory

Quasi-geostrophic theory successfully describes the mid-latitude dynamics and is widely taught in basic meteorology class. So it is necessary to derive dynamic efficiencies in Quasi-geostrophic theory. Readers might notice that we keep the turbulent fluxes in the forcing terms. It is because while turbulent fluxes are not the essentials of dynamic efficiencies, they are still very important to Quasi-geostrophic dynamics so it is better to keep them in our equations. Sec. 2.2 uses similar framework but it retains the advection of main circulation and the horizontal advection of potential temperature.

Derivation

Consider a zonally periodic, longitudally balanced flow on an β plane. The quasi-geostropic theory (App. A) gives the governing equations as

$$\text{Zonal wind:} \quad \frac{\partial \overline{u}_g}{\partial t} - f_0 \overline{v}_a = \overline{F}^*, \tag{2.1a}$$

$$\text{Geostrophic balance:} \quad \overline{u}_g = -\frac{1}{f_0}\frac{\partial \overline{\phi}}{\partial y}, \tag{2.1b}$$

$$\text{Hydrostatic:} \quad \frac{\partial \overline{\phi}}{\partial z} = \overline{b}, \tag{2.1c}$$

$$\text{Continuity:} \quad \frac{\partial \overline{v}_a}{\partial y} + \frac{\partial \rho \overline{w}}{\rho \partial z} = 0, \tag{2.1d}$$

$$\text{Thermodynamic:} \quad \frac{\partial \overline{b}}{\partial t} + \overline{w}\frac{\partial \overline{b}}{\partial z} = \frac{g}{\theta_0}\overline{Q}^*, \tag{2.1e}$$

$$\tag{2.1f}$$

where $z = (c_p\theta_0/g)[1 - (p/p_0)^\kappa]$ is the pseudo-height, $\overline{(\cdot)}$ is the zonal average, $\rho = \rho_0(p/p_0)^{(1/\kappa)-1}$ is the pseudo-density (Hoskins and Bretherton, 1972), u_g is the geostropic wind speed in zonal direction, v_a is the ageostrophic wind speed in longitudinal direction, w is the vertical components of velocity, b is the buoyancy force and ϕ is the geopotential.

By (2.1b) and (2.1c), we derive the thermal wind relation

$$f_0 \frac{\partial \overline{u}_g}{\partial z} = -\frac{\partial \overline{b}}{\partial y}. \tag{2.2}$$

After taking time derivative of (2.2), we get

$$f_0 \frac{\partial}{\partial t}\frac{\partial \overline{u}_g}{\partial z} = -\frac{\partial}{\partial t}\frac{\partial \overline{b}}{\partial y}. \tag{2.3}$$

We define

$$\text{Static stability:} \quad \rho A = \frac{\partial \overline{b}}{\partial z}, \tag{2.4a}$$

$$\text{Inertial stability:} \quad \rho C = f_0^2, \tag{2.4b}$$

to write equation (2.1a) and (2.1e) as

$$f_0 \frac{\partial \overline{u}_g}{\partial t} - \rho \overline{v}_a C = f_0 \overline{F}^*, \tag{2.5a}$$

$$\frac{\partial \overline{b}}{\partial t} + \rho \overline{w} A = \frac{g}{\theta_0} \overline{Q}^*. \tag{2.5b}$$

According to (2.1d), we define the streamfunction ψ such that

$$(\rho \overline{v}_a, \rho \overline{w}) = \left(-\frac{\partial \psi}{\partial z}, \frac{\partial \psi}{\partial y} \right). \tag{2.6}$$

After adding ∂(2.5a)$/\partial z$ and ∂(2.5b)$/\partial y$ to eliminateg time derivative with the aid of (2.3) and substituting (2.6) into it, we obtain diagnostic equation known as the Eliassen-Sawyer circulation equation

$$\mathbf{L}\psi = \frac{g}{\theta_0}\frac{\partial \overline{Q}^*}{\partial y} - f_0 \frac{\partial \overline{F}^*}{\partial z}, \tag{2.7a}$$

where

$$\mathbf{L}\,(\,\cdot\,) = \frac{\partial}{\partial y}\left(A \frac{\partial\,(\,\cdot\,)}{\partial y} \right) + \frac{\partial}{\partial z}\left(C \frac{\partial\,(\,\cdot\,)}{\partial z} \right), \tag{2.7b}$$

and is elliptic if $AC > 0$. The boundary conditions for (2.7a) are that $\psi = 0$ on top bottom, left, and right boundaries.

From a balanced system, we have the following energy equations

$$\frac{\mathrm{d}\mathbf{P}}{\mathrm{d}t} = \mathbf{H} - \mathbf{C}, \tag{2.8a}$$

$$\frac{\mathrm{d}\mathbf{K}}{\mathrm{d}t} = \mathbf{C} + \mathbf{M}, \tag{2.8b}$$

where

$$\mathbf{P} = \iint c_p \overline{T}\ \rho \mathrm{d}y\mathrm{d}z, \tag{2.9a}$$

$$\mathbf{K} = \iint \frac{\overline{u}_g^2}{2}\ \rho \mathrm{d}y\mathrm{d}z, \tag{2.9b}$$

$$\mathbf{H} = \iint c_p \Pi \overline{Q}^*\ \rho \mathrm{d}y\mathrm{d}z, \tag{2.9c}$$

$$\mathbf{C} = \iint \overline{w}\overline{b}\ \rho \mathrm{d}y\mathrm{d}z, \tag{2.9d}$$

$$\mathbf{M} = \iint \overline{F}^*\, \overline{u}_g\ \rho \mathrm{d}y\mathrm{d}z. \tag{2.9e}$$

Substituting (2.6) into (2.9d), we obtain

$$\mathbf{C} = \int \overline{b} \frac{\partial \psi}{\partial y}\, \mathrm{d}y\mathrm{d}z. \tag{2.10}$$

After integrating by parts, (2.10) becomes

$$\mathbf{C} = -\int \psi \frac{\partial \overline{b}}{\partial y}\, \mathrm{d}y\mathrm{d}z. \tag{2.11}$$

Now we define a quantity χ which satisfies

$$\mathbf{L}\chi = \frac{\partial \overline{b}}{\partial y}, \tag{2.12}$$

with the same boundary condition as (2.7a). Substituting (2.12) into (2.11) and applying self-adjoint property, we obtain

$$\mathbf{C} = -\int \psi \mathbf{L}\chi\, \mathrm{d}y\mathrm{d}z = -\int \chi \mathbf{L}\psi\, \mathrm{d}y\mathrm{d}z. \tag{2.13}$$

Substituting (2.7a) into (2.13) and integrating by parts again, we get

$$\begin{aligned} \mathbf{C} &= -\int \chi \left(\frac{g}{\theta_0} \frac{\partial \overline{Q}^*}{\partial y} - f_0 \frac{\partial \overline{F}^*}{\partial z} \right) \mathrm{d}y\mathrm{d}z \\ &= \int c_p \Pi \overline{Q}^* \eta_H\ \rho \mathrm{d}y\mathrm{d}z + \int \overline{F}^* \overline{u}_g \eta_M\ \rho \mathrm{d}y\mathrm{d}z, \end{aligned} \tag{2.14}$$

where

$$\eta_H = \frac{g}{\rho c_p \Pi \theta_0} \frac{\partial \chi}{\partial y}, \qquad (2.15a) \qquad \eta_M = -\frac{f}{\rho \overline{u}_g} \frac{\partial \chi}{\partial z}. \qquad (2.15b)$$

We refer to η_H as *dynamic efficiency of heat*, and η_M as *dynamic efficiency of momentum* which represent the conversion efficiency from potential to kinetic energy due to heating and momentum source.

If we let A and C in (2.4a) to be constants, then homogeneous part of (2.7a) becomes

$$A\frac{\partial^2 \psi}{\partial y^2} + C\frac{\partial^2 \psi}{\partial z^2} = 0. \qquad (2.16)$$

Letting

$$\psi(y, z) = \Psi(y)\,\Phi(z), \qquad (2.17)$$

plugging (2.17) into (2.16), and move functions of r and z to different sides, we obtain

$$\frac{1}{\Psi}\frac{\mathrm{d}^2\Psi}{\mathrm{d}y^2} = \frac{-1}{\Gamma^2\Phi}\frac{\mathrm{d}^2\Phi}{\mathrm{d}z^2} = \mu^2, \qquad (2.18)$$

where μ^2 is a constant (it is positive otherwise solutions on z direction would not satisfy boundary condition), and

$$\Gamma = \sqrt{\frac{A}{C}}, \qquad (2.19)$$

denoting the ratio between static stability and inertial stability.

Solving for Ψ, we obtain

$$\frac{\mathrm{d}^2\Psi}{\mathrm{d}r^2} = \mu^2\Psi, \qquad (2.20)$$

whose solution is

$$\Psi = c_1 e^{\mu y} + c_2 e^{-\mu y}. \qquad (2.21)$$

We thus define μ^{-1} as "Rossby length" (also sometimes referred to as "Rossby radius of deformation") characterizing horizontal length scale of the system.

Solving for Φ, we obtain

$$\Phi = c_1 \sin(\mu\Gamma z) + c_2 \cos(\mu\Gamma z). \qquad (2.22)$$

With $\psi = 0$ on top and bottom boundaries, we further get

$$\Phi = c_1 \sin(\mu \Gamma z), \tag{2.23}$$

and

$$\mu^{-1} = \frac{\Gamma z_\infty}{n\pi}, \tag{2.24}$$

where z_∞ is height of top boundary, and n is a non-negative integer. We again define

$$\gamma^{-1} = \frac{1}{\mu \Gamma}, \tag{2.25}$$

as "Rossby depth" characterizing vertical length scale of the system. Indeed, (2.25) can also be rewritten as

$$\frac{\gamma^{-1}}{\mu^{-1}} = \frac{1}{\Gamma}, \tag{2.26}$$

showing that the aspect ratio of the system is controlled by Γ, i.e. the ratio between static stability and inertial stability. To get more details about Γ, Schubert and McNoldy (2010) gave a great discussion about the application of Γ to tropical cyclones.

Concluding Remarks

In this section, we derive the Eliassen-Sawyer circulation equation (2.7a), dynamic efficiency of heat and momentum (2.15) for quasi-geostrophic theory. The last part of this section shows that the geometry of operator **L** is controlled by parameter Γ (2.19). This section can be compared with section 2.2 in which bacoclinity exists to get deeper insight.

2.2 Efficiency in Cartesian Coordinates

Cartesian coordinates is suitable for discussing physics without dealing with geometry factor. The difference between this section and Sec. 2.1 is that we retain the advection of main circulation and the horizontal advection of potential temperature, hence keeping the effect of baroclinity on the secondary circulation.

Derivation

Consider a zonally symmetric, longitudinally balanced flow on an f plane. The governing equations are given as

$$\text{Zonal wind:} \quad \frac{\mathrm{d}u}{\mathrm{d}t} - fv = F, \tag{2.27a}$$

$$\text{Logitudinal wind:} \quad fu = -\frac{\partial \phi}{\partial y}, \tag{2.27b}$$

$$\text{Hydrostatic:} \quad \frac{\partial \phi}{\partial z} = \frac{\theta}{\theta_0} g, \tag{2.27c}$$

$$\text{Continuity:} \quad \frac{\partial v}{\partial y} + \frac{\partial \rho w}{\rho \partial z} = 0, \tag{2.27d}$$

$$\text{Thermodynamic:} \quad \frac{\mathrm{d}\theta}{\mathrm{d}t} = Q, \tag{2.27e}$$

where $z = (c_p \theta_0 / g)[1 - (p/p_0)^{\kappa}]$ is the pseudo-height, $\rho = \rho_0 (p/p_0)^{(1/\kappa)-1}$ is the pseudo-density (Hoskins and Bretherton, 1972), u, v, w are the zonal, longitudinal, and vertical components of velocity, θ is the potential temperature, ϕ is the geopotential, F is the external force on zonal wind, and Q is the diabatic heating.

Noticing that $v = \mathrm{d}y/\mathrm{d}t$, (2.27a) becomes

$$\frac{\mathrm{d}u}{\mathrm{d}t} - fv = \frac{\mathrm{d}}{\mathrm{d}t}(u - fy) = \frac{\mathrm{d}u^*}{\mathrm{d}t}, \tag{2.28}$$

where $u^* = u - fy$ is the transformed zonal wind, a technique similar to "semi-geostrophic coordinate" in Hoskins and West (1979). Substituting (2.28) into (2.27b), we get

$$fu = f(u^* + fy) = -\frac{\partial \phi}{\partial y}. \tag{2.29}$$

Expanding total derivative, governing equations become

$$\text{Absolute angular mometnum:} \quad \frac{\partial u^*}{\partial t} + v\frac{\partial u^*}{\partial y} + w\frac{\partial u^*}{\partial z} = F, \tag{2.30a}$$

$$\text{Gradient wind balance:} \quad f\left(u^* + fy\right) = -\frac{\partial \phi}{\partial y}, \tag{2.30b}$$

$$\text{Hydrostatic:} \quad \frac{\partial \phi}{\partial z} = \frac{\theta}{\theta_0} g, \tag{2.30c}$$

$$\text{Continuity:} \quad \frac{\partial v}{\partial y} + \frac{\partial \rho w}{\rho \partial z} = 0, \tag{2.30d}$$

$$\text{Thermodynamic:} \quad \frac{\partial \theta}{\partial t} + v\frac{\partial \theta}{\partial y} + w\frac{\partial \theta}{\partial z} = Q, \tag{2.30e}$$

By (2.30b) and (2.30c), we derive the thermal wind relation

$$f\frac{\partial u^*}{\partial z} = -\frac{g}{\theta_0}\frac{\partial \theta}{\partial y}. \tag{2.31}$$

After taking time derivative of (2.31), we get

$$f\frac{\partial}{\partial t}\frac{\partial u^*}{\partial z} = -\frac{g}{\theta_0}\frac{\partial}{\partial t}\frac{\partial \theta}{\partial y}. \tag{2.32}$$

We define

$$\text{Static stability:} \quad \rho A = \frac{g}{\theta_0}\frac{\partial \theta}{\partial z}, \tag{2.33a}$$

$$\text{Baroclinity:} \quad \rho B = -\frac{g}{\theta_0}\frac{\partial \theta}{\partial y} = f\frac{\partial u^*}{\partial z}, \tag{2.33b}$$

$$\text{Inertial stability} \quad \rho C = -f\frac{\partial u^*}{\partial y}, \tag{2.33c}$$

to rewrite equation (2.30a) and (2.30e) as

$$f\frac{\partial u^*}{\partial t} - \rho v C + \rho w B = fF, \tag{2.34a}$$

$$\frac{g}{\theta_0}\frac{\partial \theta}{\partial t} - \rho v B + \rho w A = \frac{g}{\theta_0} Q. \tag{2.34b}$$

According to (2.30d), we define the streamfunction ψ such that

$$(\rho v, \rho w) = \left(-\frac{\partial \psi}{\partial z}, \frac{\partial \psi}{\partial y} \right). \tag{2.35}$$

After adding ∂(2.34a)$/\partial z$ and ∂(2.34b) to eliminate time derivative with the aid of (2.32) and substituting (2.35) into it, we obtain the diagnostic equation known as the Eliassen-Sawyer circulation equation

$$\mathbf{L}\psi = \frac{g}{\theta_0}\frac{\partial Q}{\partial y} + f\frac{\partial F}{\partial z}, \tag{2.36a}$$

where

$$\mathbf{L}\,(\,\cdot\,) = \frac{\partial}{\partial y}\left(A\frac{\partial\,(\,\cdot\,)}{\partial y} + B\frac{\partial\,(\,\cdot\,)}{\partial z} \right) + \frac{\partial}{\partial z}\left(B\frac{\partial\,(\,\cdot\,)}{\partial y} + C\frac{\partial\,(\,\cdot\,)}{\partial z} \right), \tag{2.36b}$$

and is elliptic if $B^2 - AC < 0$. The boundary conditions for (2.36a) are that $\psi = 0$ on top, bottom, left, and right boundaries.

From a balanced system, we have the following energy equations

$$\frac{\mathrm{d}\mathbf{P}}{\mathrm{d}t} = \mathbf{H} - \mathbf{C}, \tag{2.37a}$$

$$\frac{\mathrm{d}\mathbf{K}}{\mathrm{d}t} = \mathbf{C} + \mathbf{M}, \tag{2.37b}$$

where

$$\mathbf{P} = \iint c_p T\ \rho \mathrm{d}y\mathrm{d}z, \tag{2.38a}$$

$$\mathbf{K} = \iint \frac{u^2}{2}\ \rho \mathrm{d}y\mathrm{d}z, \tag{2.38b}$$

$$\mathbf{H} = \iint c_p \Pi Q\ \rho \mathrm{d}y\mathrm{d}z, \tag{2.38c}$$

$$\mathbf{C} = \iint \frac{g}{\theta_0}\theta w\ \rho \mathrm{d}y\mathrm{d}z, \tag{2.38d}$$

$$\mathbf{M} = \iint Fu\ \rho \mathrm{d}y\mathrm{d}z. \tag{2.38e}$$

Substituting (2.35) into (2.38d), we obtain

$$\mathbf{C} = \iint \theta\frac{g}{\theta_0}\frac{\partial \psi}{\partial y}\ \mathrm{d}y\mathrm{d}z. \tag{2.39}$$

After integrating by parts, (2.39) becomes

$$\mathbf{C} = -\int \psi \frac{g}{\theta_0}\frac{\partial \theta}{\partial y}\,\mathrm{d}y\mathrm{d}z. \tag{2.40}$$

Now we define a quantity χ which satisfies

$$\mathbf{L}\chi = \frac{g}{\theta_0}\frac{\partial \theta}{\partial y}, \tag{2.41}$$

with the same boundary condition as (2.36a). Substituting (2.41) into (2.40) and applying self-adjoint property, we obtain

$$\mathbf{C} = -\int \psi \mathbf{L}\chi\,\mathrm{d}y\mathrm{d}z = -\int \chi \mathbf{L}\psi\,\mathrm{d}y\mathrm{d}z. \tag{2.42}$$

Substituting (2.36a) into (2.42) and integrating by parts again, we get

$$\begin{aligned}\mathbf{C} &= -\int \chi\left(\frac{g}{\theta_0}\frac{\partial Q}{\partial y} + f\frac{\partial F}{\partial z}\right)\mathrm{d}y\mathrm{d}z \\ &= \int c_p \Pi Q \eta_H\,\rho\mathrm{d}y\mathrm{d}z + \int Fu\eta_M\,\rho\mathrm{d}y\mathrm{d}z,\end{aligned} \tag{2.43}$$

where

$$\eta_H = \frac{g}{\rho c_p \Pi \theta_0}\frac{\partial \chi}{\partial y}, \tag{2.44a}$$

$$\eta_M = \frac{f}{\rho u}\frac{\partial \chi}{\partial z}. \tag{2.44b}$$

We refer to η_H as *dynamic efficiency of heat*, and η_M as *dynamic efficiency of momentum* which represent the conversion efficiency from potential to kinetic energy due to heating and momentum source.

If we let A and C in (2.33a) to be constants, $B = 0$, then homogeneous part of (2.36a) becomes

$$A\frac{\partial^2 \psi}{\partial y^2} + C\frac{\partial^2 \psi}{\partial z^2} = 0. \tag{2.45}$$

Letting

$$\psi(y,z) = \Psi(y)\,\Phi(z), \tag{2.46}$$

plugging (2.46) into (2.45), and move functions of r and z to different sides, we obtain

$$\frac{1}{\Psi}\frac{\mathrm{d}^2\Psi}{\mathrm{d}y^2} = \frac{-1}{\Gamma^2\Phi}\frac{\mathrm{d}^2\Phi}{\mathrm{d}z^2} = \mu^2, \tag{2.47}$$

where μ^2 is a constant (it is positive otherwise solutions on z direction would not satisfy boundary condition), and

$$\Gamma = \sqrt{\frac{A}{C}}, \tag{2.48}$$

denoting the ratio between static stability and inertial stability..

Solving for Ψ, we obtain

$$\frac{\mathrm{d}^2\Psi}{\mathrm{d}r^2} = \mu^2\Psi, \tag{2.49}$$

whose solution is

$$\Psi = c_1 e^{\mu y} + c_2 e^{-\mu y}. \tag{2.50}$$

We thus define μ^{-1} as "Rossby length" (also sometimes referred to as "Rossby radius of deformation") characterizing horizontal length scale of the system.

Solving for Φ, we obtain

$$\Phi = c_1 \sin(\mu\Gamma z) + c_2 \cos(\mu\Gamma z). \tag{2.51}$$

With $\psi = 0$ on top and bottom boundaries, we further get

$$\Phi = c_1 \sin(\mu\Gamma z), \tag{2.52}$$

and

$$\mu^{-1} = \frac{\Gamma z_\infty}{n\pi}, \tag{2.53}$$

where z_∞ is height of top boundary, and n is a non-negative integer. We again define

$$\gamma^{-1} = \frac{1}{\mu\Gamma}, \tag{2.54}$$

as "Rossby depth" characterizing vertical length scale of the system. Indeed, (2.54) can

also be rewritten as

$$\frac{\gamma^{-1}}{\mu^{-1}} = \frac{1}{\Gamma}, \tag{2.55}$$

showing that the aspect ratio of the system is controlled by Γ, i.e. the ratio between static stability and inertial stability. To get more details about Γ, Schubert and McNoldy (2010) gave a great discussion about the application of Γ to tropical cyclones.

Concluding Remarks

In this section, we derive the Eliassen-Sawyer circulation equation (2.36a), dynamic efficiency of heat and momentum (2.44) for Cartesian coordinates. The last part of this section shows that the geometry of operator **L** is controlled by parameter Γ (2.48). When compared with Sec. 2.1, the main difference is the existence of baroclinity B in (2.36a) because we retain the vertical advection of zonal wind and horizontal advection of temperature (or buoyancy in Sec. 2.1). In general, baroclinity makes little difference since A and C are usually much more significant than B.

2.3 Efficiency in Cylindrical Coordinates

Cylindrical coordinates is suitable to deal with any rotation system on a plane, and TC problems use this coordinates intensively. Schubert and Hack (1982) gave a different perspective other than CISK to emphasis on the dynamical structure of a vortex which enhances the warming of the core. Hack et al. (1989) used dynamic efficiency of heat to point out the importance of horizontal structure of heating. Rozoff et al. (2008) discussed the effect of a contracting and intensifying concentric eyewall.

Another fact is that governing equations in cylindrical coordinates and spherical coordinates are conceptually the same. The linkage between them will be elaborated more in App. D.

Derivation

Consider an axisymmetric, balanced flow on an f plane. The governing equations are given as

$$\text{Radial wind:} \quad \frac{\partial \phi}{\partial r} = fv + \frac{v^2}{r}, \tag{2.56a}$$

$$\text{Tangential wind:} \quad \frac{\mathrm{d}v}{\mathrm{d}t} = -fu - \frac{uv}{r} + F, \tag{2.56b}$$

$$\text{Hydrostatic:} \quad \frac{\partial \phi}{\partial z} = \frac{\theta}{\theta_0} g, \tag{2.56c}$$

$$\text{Continuity:} \quad \frac{\partial ru}{r\partial r} + \frac{\partial \rho w}{\rho \partial z} = 0, \tag{2.56d}$$

$$\text{Thermodynamic:} \quad \frac{\mathrm{d}\theta}{\mathrm{d}t} = Q, \tag{2.56e}$$

where $z = (c_p\theta_0/g)[1 - (p/p_0)^\kappa]$ is the pseudo-height, $\rho = \rho_0(p/p_0)^{(1/\kappa)-1}$ is the pseudo-density (Hoskins and Bretherton, 1972), u, v, w are the radial, tangential, and vertical components of velocity, θ is the potential temperature, ϕ is the geopotential, F is external force on tangential wind, and Q is the diabatic heating.

Noticing that $u = \mathrm{d}r/\mathrm{d}t$, we multiply (2.56b) by r to get

$$r\frac{\mathrm{d}v}{\mathrm{d}t} + \frac{\mathrm{d}u}{\mathrm{d}t}v + f\frac{\mathrm{d}r}{\mathrm{d}t} = \frac{\mathrm{d}}{\mathrm{d}t}\left(rv + \frac{1}{2}fr^2\right) = \frac{\mathrm{d}m}{\mathrm{d}t}, \tag{2.57}$$

where $m = rv + 1/2fr^2$ is the absolute angular momentum. Substituting (2.57) into (2.56a), we get

$$\begin{aligned} fv + \frac{v^2}{r} &= \frac{1}{r^2}v\left(rv + fr^2\right) \\ &= \frac{1}{r^3}\left(rv + \frac{1}{2}fr^2 - \frac{1}{2}fr^2\right)\left(rv + \frac{1}{2}fr^2 + \frac{1}{2}fr^2\right) \\ &= \frac{1}{r^3}\left(m^2 - \frac{1}{4}f^2r^4\right). \end{aligned} \tag{2.58}$$

Expanding total derivative, governing equations become

$$\text{Radial wind:} \quad \frac{\partial\phi}{\partial r} = \frac{1}{r^3}\left(m^2 - \frac{1}{4}f^2r^4\right), \tag{2.59a}$$

$$\text{Absolute angular momentum:} \quad \frac{\partial m}{\partial t} + u\frac{\partial m}{\partial r} + w\frac{\partial m}{\partial z} = rF, \tag{2.59b}$$

$$\text{Hydrostatic:} \quad \frac{\partial\phi}{\partial z} = \frac{\theta}{\theta_0}g, \tag{2.59c}$$

$$\text{Continuity:} \quad \frac{\partial ru}{r\partial r} + \frac{\partial\rho w}{\rho\partial z} = 0, \tag{2.59d}$$

$$\text{Thermodynamic:} \quad \frac{\partial\theta}{\partial t} + u\frac{\partial\theta}{\partial r} + w\frac{\partial\theta}{\partial z} = Q. \tag{2.59e}$$

By (2.59a) and (2.59c), we derive the thermal wind relation

$$\frac{g}{\theta_0}\frac{\partial\theta}{\partial r} = \frac{1}{r^3}\frac{\partial m^2}{\partial z}. \tag{2.60}$$

After taking time derivative of (2.60), we get

$$\frac{\partial}{\partial t}\frac{g}{\theta_0}\frac{\partial\theta}{\partial r} = \frac{\partial}{\partial t}\frac{1}{r^3}\frac{\partial m^2}{\partial z}. \tag{2.61}$$

We define

$$\text{Static stability:} \quad \rho A = \frac{g}{\theta_0}\frac{\partial \theta}{\partial z}, \tag{2.62a}$$

$$\text{Baroclinity:} \quad \rho B = -\frac{g}{\theta_0}\frac{\partial \theta}{\partial r} = -\frac{1}{r^3}\frac{\partial m^2}{\partial z}, \tag{2.62b}$$

$$\text{Inertial stability:} \quad \rho C = \frac{1}{r^3}\frac{\partial m^2}{\partial r}, \tag{2.62c}$$

to rewrite (2.59b) and (2.59e) as

$$\frac{1}{r^3}\frac{\partial m^2}{\partial t} + \rho u C - \rho w B = \frac{2mF}{r^2}, \tag{2.63a}$$

$$\frac{g}{\theta_0}\frac{\partial \theta}{\partial t} - \rho u B + \rho w A = \frac{g}{\theta_0} Q. \tag{2.63b}$$

According to (2.59d) we define the streamfunction ψ such that

$$(\rho u, \rho w) = \left(-\frac{\partial \psi}{\partial z}, \frac{\partial r\psi}{r\partial r} \right). \tag{2.64}$$

After subtracting ∂(2.63b)$/\partial r$ from ∂(2.63a)$/\partial z$ to eliminate partial derivative of time with the aid of (2.61) and substituting (2.64) into it, we obtain the diagnostic equation known as the Eliassen-Sawyer circulation equation

$$\mathbf{L}\psi = \frac{g}{\theta_0}\frac{\partial Q}{\partial r} - \frac{1}{r^2}\frac{\partial 2mF}{\partial z}, \tag{2.65a}$$

where

$$\mathbf{L}\left(\,\cdot\,\right) = \frac{\partial}{\partial r}\left(A\frac{\partial r\left(\,\cdot\,\right)}{\partial r} r + B\frac{\partial\left(\,\cdot\,\right)}{\partial z} \right) + \frac{\partial}{\partial z}\left(B\frac{\partial r\left(\,\cdot\,\right)}{r\partial r} + C\frac{\partial\left(\,\cdot\,\right)}{\partial z} \right), \tag{2.65b}$$

and (2.65b) is elliptic if $B^2 - AC < 0$. The boundary conditions for (2.65a) are that $\psi = 0$ on top, bottom, and inner boundaries and $\psi \to 0$ as $r \to \infty$.

From a balanced vortex system, we can derive the following energy equations

$$\frac{\mathrm{d}\mathbf{P}}{\mathrm{d}t} = \mathbf{H} - \mathbf{C}, \tag{2.66a}$$

$$\frac{\mathrm{d}\mathbf{K}}{\mathrm{d}t} = \mathbf{C} + \mathbf{M}, \tag{2.66b}$$

where

$$\mathbf{P} = \iint c_p T \ \rho r \mathrm{d}r\mathrm{d}z, \tag{2.67a}$$

$$\mathbf{K} = \iint \frac{v^2}{2} \ \rho r \mathrm{d}r\mathrm{d}z, \tag{2.67b}$$

$$\mathbf{H} = \iint c_p \Pi Q \ \rho r \mathrm{d}r\mathrm{d}z, \tag{2.67c}$$

$$\mathbf{C} = \iint \frac{g}{\theta_0} w\theta \ \rho r \mathrm{d}r\mathrm{d}z, \tag{2.67d}$$

$$\mathbf{M} = \iint Fv \ \rho \mathrm{d}r\mathrm{d}z. \tag{2.67e}$$

Substituting (2.64) into (2.67d), we obtain

$$\mathbf{C} = \iint \theta \frac{g}{\theta_0} \frac{\partial r\psi}{\partial r} \ \mathrm{d}r\mathrm{d}z. \tag{2.68}$$

After integrating by parts, (2.68) becomes

$$\mathbf{C} = -\iint \psi \frac{g}{\theta_0} \frac{\partial \theta}{\partial r} \ r\mathrm{d}r\mathrm{d}z. \tag{2.69}$$

Now we define a quantity χ which satisfies

$$\mathbf{L}\chi = \frac{g}{\theta_0} \frac{\partial \theta}{\partial r}, \tag{2.70}$$

with the same boundary condition as (2.65a). Substituting (2.70) into (2.69) and applying self-adjoint property, we obtain

$$\mathbf{C} = -\iint \psi \mathbf{L}\chi \ r\mathrm{d}r\mathrm{d}z = -\iint \chi \mathbf{L}\psi \ r\mathrm{d}r\mathrm{d}z. \tag{2.71}$$

Substituting (2.65a) into (2.71) and integrating by parts again, we get

$$\begin{aligned} \mathbf{C} &= -\iint \frac{g}{\theta_0} \frac{\partial Q}{\partial r} - \frac{1}{r^2} \frac{\partial 2mF}{\partial z} \ r\mathrm{d}r\mathrm{d}z \\ &= \iint Q c_p \Pi \eta_H \ \rho r \mathrm{d}r\mathrm{d}z + \iint Fv\eta_M \ \rho r \mathrm{d}r\mathrm{d}z, \end{aligned} \tag{2.72}$$

where

$$\eta_H = \frac{g}{\rho c_p \Pi \theta_0} \frac{\partial r\chi}{r\partial r}, \tag{2.73a}$$

$$\eta_M = -\frac{2m}{\rho v r^2} \frac{\partial \chi}{\partial z}. \tag{2.73b}$$

We refer to η_H as *dynamic efficiency of heat*, and η_M as *dynamic efficiency of momentum* which represent the conversion efficiency from potential to kinetic energy due to heating and momentum source.

If we let A and C in (2.62) to be constants, $B = 0$, then homogeneous part of (2.65a) becomes

$$\frac{\partial}{\partial r}\left(\frac{\partial r\psi}{r\partial r}\right) + \frac{1}{\Gamma}\frac{\partial^2\psi}{\partial z^2} = 0. \tag{2.74}$$

Letting

$$\psi(r,z) = \Psi(r)\,\Phi(z), \tag{2.75}$$

plugging (2.75) into (2.74), and move functions of r and z to different sides, we obtain

$$\frac{1}{\Psi}\left(\frac{\mathrm{d}^2\Psi}{\mathrm{d}r^2} + \frac{1}{r}\frac{\mathrm{d}\Psi}{\mathrm{d}r} - \frac{1}{r^2}\Psi\right) = \frac{-1}{\Gamma^2\Phi}\frac{\mathrm{d}^2\Phi}{\mathrm{d}z^2} = \mu^2 \tag{2.76}$$

where μ^2 is a constant.

Solving for Ψ, we obtain

$$r^2\frac{\mathrm{d}^2\Psi}{\mathrm{d}r^2} + r\frac{\mathrm{d}\Psi}{\mathrm{d}r} + \Psi\left(1+\mu^2r^2\right) = 0, \tag{2.77}$$

which is modified Bessel's differential equation. We thus define μ^{-1} as "Rossby length" (also sometimes referred to as "Rossby radius of deformation") characterizing horizontal length scale of the system.

Solving for Φ, we obtain

$$\Phi = c_1\sin(\mu\Gamma z) + c_2\cos(\mu\Gamma z). \tag{2.78}$$

With $\psi = 0$ on top and bottom boundaries, we further get

$$\Phi = c_1\sin(\mu\Gamma z), \tag{2.79}$$

and

$$\mu^{-1} = \frac{\Gamma z_\infty}{n\pi}, \tag{2.80}$$

where z_∞ is height of top boundary, and n is a non-negative integer. We again define

$$\gamma^{-1} = \frac{1}{\mu\Gamma}, \tag{2.81}$$

as "Rossby depth" characterizing vertical length scale of the system. Indeed, (2.81) can also be rewritten as

$$\frac{\gamma^{-1}}{\mu^{-1}} = \frac{1}{\Gamma}, \tag{2.82}$$

showing that the aspect ratio of the system is controlled by Γ, i.e. the ratio between static stability and inertial stability.

Concluding Remarks

In this section, we derive the Eliassen-Sawyer circulation equation (2.65a), dynamic efficiency of heat and momentum (2.73) for cylindrical coordinates. The last part of this section shows that the geometry of operator $\mathbf{L}$ is controlled by parameter Γ (2.81). Notice that the efficiency of heat involves horizontal geometry, so efficiency of heat must be sensitive to its position in radial direction. This might suggest that TC's properties may change rapidly when its heating position fluctuates radially in small radius.

2.4 Efficiency in Spherical Coordinates

Spherical coordinates can be used when dealing with planetary scale problem. For example, Hack et al. (1989) explained why the Hadley cell is stronger in the winter hemisphere, Schubert et al. (1989) studied the trade-wind inversion to enlight problem from subtropical latitude to tropics.

Another fact is that governing equations in spherical coordinates and cylindrical coordinates are conceptually the same. The linkage between them will be elaborated more in App. D.

Derivation

Consider an axisymmetric, balanced flow on a sphere. The governing equations are given as

$$\text{Absolute angular momentum:} \quad \frac{\partial m}{\partial t} + v\frac{\partial m}{\partial (a\phi)} + w\frac{\partial m}{\partial z} = RF, \tag{2.83a}$$

$$\text{Longitudinal wind:} \quad \frac{\sin\phi}{R^3}\left(m^2 - \Omega^2 R^4\right) = -\frac{\partial G}{\partial (a\phi)}, \tag{2.83b}$$

$$\text{Hydrostatic:} \quad \frac{\partial G}{\partial z} = \frac{\theta}{\theta_0} g, \tag{2.83c}$$

$$\text{Continuity:} \quad \frac{\partial Rv}{R\partial (a\phi)} + \frac{\partial \rho w}{\rho \partial z} = 0, \tag{2.83d}$$

$$\text{Thermodynamic:} \quad \frac{\partial \theta}{\partial t} + v\frac{\partial \theta}{\partial (a\phi)} + w\frac{\partial \theta}{\partial z} = Q, \tag{2.83e}$$

where a is the radius of Earth, ϕ is the latitude, $R = a\cos\phi$ is the radius relative to the rotation axis, $z = (c_p\theta_0/g)[1 - (p/p_0)^\kappa]$ is the pseudo-height, $m = Ru + \Omega R^2$ is the absolute angular momentum, $\rho = \rho_0(p/p_0)^{(1/\kappa)-1}$ is the pseudo-density (Hoskins and Bretherton, 1972), u, v, w are the zonal, longitudinal, and radial components of velocity, θ is the potential temperature, G is the geopotential, F is external force on zonal wind, and Q is the diabatic heating.

By (2.83b) and (2.83c), we derive the thermal wind relation

$$\frac{g}{\theta_0}\frac{\partial\theta}{\partial(a\phi)} = \frac{-\sin\phi}{R^3}\frac{\partial m^2}{\partial z}. \tag{2.84}$$

After taking time derivative of (2.84), we get

$$\frac{g}{\theta_0}\frac{\partial}{\partial t}\frac{\partial\theta}{\partial(a\phi)} = \frac{-\sin\phi}{R^3}\frac{\partial}{\partial t}\frac{\partial m^2}{\partial z}. \tag{2.85}$$

We define

$$\text{Static stability:} \quad \rho A = \frac{g}{\theta_0}\frac{\partial\theta}{\partial z}, \tag{2.86a}$$

$$\text{Baroclinity:} \quad \rho B = -\frac{g}{\theta_0}\frac{\partial\theta}{\partial(a\phi)} = \frac{\sin\phi}{R^3}\frac{\partial m^2}{\partial z}, \tag{2.86b}$$

$$\text{Inertial stability:} \quad \rho C = -\frac{\sin\phi}{R^3}\frac{\partial m^2}{\partial(a\phi)}, \tag{2.86c}$$

to rewrite (2.83a) and (2.83e) as

$$\frac{\sin\phi}{R^3}\frac{\partial m^2}{\partial t} - \rho v C + \rho w B = \frac{\sin\phi}{R^2}2mF \tag{2.87a}$$

$$\frac{g}{\theta_0}\frac{\partial\theta}{\partial t} - \rho v B + \rho w A = \frac{g}{\theta_0}Q \tag{2.87b}$$

Notice that since $m = 0$ on $\phi = \pm\pi/2$ (north and south pole), the following integral

$$\int_{\phi=-\pi/2}^{\pi/2} -\frac{\rho C R^3}{\sin\phi}\mathrm{d}(a\phi) = \left(m^2\right)\Big|_{\phi=-\pi/2}^{\pi/2} = 0, \tag{2.88}$$

must be satisfied.

According to (2.83d) we define the streamfunction ψ such that

$$(\rho v, \rho w) = \left(-\frac{\partial\psi}{\partial z}, \frac{\partial R\psi}{R\partial(a\phi)}\right) \tag{2.89}$$

After adding ∂(2.87a)$/\partial z$ and ∂(2.87b)$/\partial(a\phi)$ to eliminate partial derivative of time with the aid of (2.85) and substituting (2.89) into it, we obtain the diagnostic equation known

as the Eliassen-Sawyer circulation equation

$$\mathbf{L}\psi = \frac{g}{\theta_0}\frac{\partial Q}{\partial(a\phi)} + \frac{\sin\phi}{R^2}\frac{\partial\, 2mF}{\partial z}, \tag{2.90a}$$

where

$$\mathbf{L}\,(\,\cdot\,) = \frac{\partial}{\partial(a\phi)}\left(A\frac{\partial R\,(\,\cdot\,)}{R\partial(a\phi)} + B\frac{\partial\,(\,\cdot\,)}{\partial z}\right) + \frac{\partial}{\partial z}\left(B\frac{\partial R\,(\,\cdot\,)}{R\partial(a\phi)} + C\frac{\partial\,(\,\cdot\,)}{\partial z}\right), \tag{2.90b}$$

and (2.90b) is elliptic if $B^2 - AC < 0$. The boundary conditions for (2.65a) are that $\psi = 0$ on top, bottom, inner, and outer boundaries.

From a balanced vortex system, we can derive the following energy equations

$$\frac{\mathrm{d}\mathbf{P}}{\mathrm{d}t} = \mathbf{H} - \mathbf{C}, \tag{2.91a}$$

$$\frac{\mathrm{d}\mathbf{K}}{\mathrm{d}t} = \mathbf{C} + \mathbf{M}, \tag{2.91b}$$

where

$$\mathbf{P} = \iint c_p T\ \rho R\mathrm{d}(a\phi)\,\mathrm{d}z, \tag{2.92a}$$

$$\mathbf{K} = \iint \frac{u^2}{2}\ \rho R\mathrm{d}(a\phi)\,\mathrm{d}z, \tag{2.92b}$$

$$\mathbf{H} = \iint c_p \Pi Q\ \rho R\mathrm{d}(a\phi)\,\mathrm{d}z, \tag{2.92c}$$

$$\mathbf{C} = \iint \frac{g}{\theta_0} w\theta\ \rho R\mathrm{d}(a\phi)\,\mathrm{d}z, \tag{2.92d}$$

$$\mathbf{M} = \iint Fv\ \rho R\mathrm{d}(a\phi)\,\mathrm{d}z. \tag{2.92e}$$

Substituting (2.89) into (2.92d), we obtain

$$\mathbf{C} = \iint \theta\frac{g}{\theta_0}\frac{\partial R\psi}{\partial(a\phi)}\ \mathrm{d}(a\phi)\,\mathrm{d}z. \tag{2.93}$$

After integrating by parts, (2.93) becomes

$$\mathbf{C} = -\iint \psi\frac{g}{\theta_0}\frac{\partial\theta}{\partial(a\phi)}\ R\mathrm{d}(a\phi)\,\mathrm{d}z. \tag{2.94}$$

Now we define a quantity χ which satisfies

$$\mathbf{L}\chi = \frac{g}{\theta_0}\frac{\partial\theta}{\partial(a\phi)}, \tag{2.95}$$

with the same boundary condition as (2.90a). Substituting (2.95) into (2.94) and applying

self-adjoint property, we obtain

$$\mathbf{C} = -\iint \psi \mathbf{L}\chi \; R\mathrm{d}(a\phi)\,\mathrm{d}z = -\iint \chi \mathbf{L}\psi \; R\mathrm{d}(a\phi)\,\mathrm{d}z. \tag{2.96}$$

Substituting (2.90a) into (2.96) and integrating by parts again, we get

$$\begin{aligned}\mathbf{C} &= -\iint \frac{g}{\theta_0}\frac{\partial Q}{\partial(a\phi)} + \frac{\sin\phi}{R^2}\frac{\partial\, 2mF}{\partial z}\; R\mathrm{d}(a\phi)\,\mathrm{d}z \\ &= \iint c_p \Pi Q \eta_H \; \rho R\mathrm{d}(a\phi)\,\mathrm{d}z + \iint Fu\eta_M \; \rho R\mathrm{d}(a\phi)\,\mathrm{d}z,\end{aligned} \tag{2.97}$$

where

$$\eta_H = \frac{g}{\rho c_p \Pi \theta_0}\frac{\partial R\chi}{R\partial(a\phi)}, \tag{2.98a}$$

$$\eta_M = \frac{2m\sin\phi}{\rho u R^2}\frac{\partial \chi}{\partial z}. \tag{2.98b}$$

We refer to η_H as *dynamic efficiency of heat*, and η_M as *dynamic efficiency of momentum* which represent the conversion efficiency from potential to kinetic energy due to heating and momentum source.

Concluding Remarks

In this section, we derive the Eliassen-Sawyer circulation equation (2.90a), dynamic efficiency of heat and momentum (2.98) for spherical coordinates. This coordinates is widely applied to study large-scale dynamics.

2.5 Efficiency in Shallow Water Model

The linear shallow water equations an be view as a vertical mode of the linearized primitive equations. This implies the essentials of dynamic efficiencies lies in the horizontal structure of the rotating system.

Derivation

Consider an axisymmetric, balanced flow on an f plane. The governing equations are given as

$$\text{Radial flow:} \quad g\frac{\partial h}{\partial r} = fv + \frac{v^2}{r}, \tag{2.99a}$$

$$\text{Tangential flow:} \quad \frac{\mathrm{d}v}{\mathrm{d}t} = -fu - \frac{uv}{r} + F, \tag{2.99b}$$

$$\text{Continuity:} \quad \frac{\partial h}{\partial t} + \frac{\partial hru}{r\partial r} = Q, \tag{2.99c}$$

where u, v are the radial, and tangential component of velocity, h is the height of the surface, and F is the external force on tangential flow.

Noticing that $u = \mathrm{d}r/\mathrm{d}t$, we multiply (2.99b) by r to get

$$r\frac{\mathrm{d}v}{\mathrm{d}t} + \frac{\mathrm{d}u}{\mathrm{d}t}v + f\frac{\mathrm{d}r}{\mathrm{d}t} = \frac{\mathrm{d}}{\mathrm{d}t}\left(rv + \frac{1}{2}fr^2\right) = \frac{\mathrm{d}m}{\mathrm{d}t}, \tag{2.100}$$

where $m = rv + 1/2fr^2$ is the absolute angular momentum. Substituting (2.100) into (2.99b), we get

$$\begin{aligned} fv + \frac{v^2}{r} &= \frac{1}{r^2}v\left(rv + fr^2\right) \\ &= \frac{1}{r^3}\left(rv + \frac{1}{2}fr^2 - \frac{1}{2}fr^2\right)\left(rv + \frac{1}{2}fr^2 + \frac{1}{2}fr^2\right) \\ &= \frac{1}{r^3}\left(m^2 - \frac{1}{4}f^2r^4\right). \end{aligned} \tag{2.101}$$

Expanding total derivative, governing equations become

$$\text{Radial flow:} \quad g\frac{\partial h}{\partial r} = \frac{1}{r^3}\left(m^2 - \frac{1}{4}f^2r^4\right), \tag{2.102a}$$

$$\text{Angular momentum:} \quad \frac{\partial m}{\partial t} + u\frac{\partial m}{\partial r} = rF, \tag{2.102b}$$

$$\text{Continuity:} \quad \frac{\partial h}{\partial t} + \frac{\partial hru}{r\partial r} = Q. \tag{2.102c}$$

After taking time derivative of (2.102a), we get

$$g\frac{\partial}{\partial t}\frac{\partial h}{\partial r} = \frac{1}{r^3}\frac{\partial m^2}{\partial t}. \tag{2.103}$$

We define

$$\text{Inertial stability:} \quad ghC = \frac{\partial m^2}{r^3\partial r}, \tag{2.104}$$

to rewrite (2.102b) and (2.102c) as

$$\frac{1}{r^3}\frac{\partial m^2}{\partial t} + ghuC = \frac{2mF}{r^2}, \tag{2.105a}$$

$$g\frac{\partial h}{\partial t} + g\frac{\partial rhu}{r\partial r} = gQ. \tag{2.105b}$$

We define a variable ψ as

$$\psi = uh. \tag{2.106}$$

After subtracting ∂(2.105b)$/\partial r$ from (2.105a) to eliminate time derivative with the ad of (2.103) and substituting (2.106) into it, we obtain the diagnostic equation

$$\mathbf{L}\psi = \frac{\partial Q}{\partial r} - \frac{2mF}{gr^2}, \tag{2.107a}$$

where

$$\mathbf{L}\left(\,\cdot\,\right) = \frac{\partial}{\partial r}\left(\frac{\partial r\left(\,\cdot\,\right)}{r\partial r}\right) - C\left(\,\cdot\,\right), \tag{2.107b}$$

and boundary conditions for (2.107a) are that $\psi = 0$ on inner boundary and $\psi \to 0$ as

$r \to \infty$.

From a balanced vortex system, we can derive the following energy equations

$$\frac{\mathrm{d}\mathbf{P}}{\mathrm{d}t} = \mathbf{H} - \mathbf{C}, \qquad (2.108a) \qquad \frac{\mathrm{d}\mathbf{K}}{\mathrm{d}t} = \mathbf{C} + \mathbf{M}, \qquad (2.108b)$$

where

$$\mathbf{P} = \int g\frac{h^2}{2}\, r\mathrm{d}r, \qquad (2.109a) \qquad \mathbf{H} = \int gQ\, hr\mathrm{d}r, \qquad (2.109c)$$

$$\mathbf{K} = \int \frac{v^2}{2}\, hr\mathrm{d}r, \qquad (2.109b) \qquad \mathbf{C} = -\int gh\frac{\partial ruh}{\partial r}\, \mathrm{d}r, \qquad (2.109d)$$

$$\mathbf{M} = \int Fvh\, r\mathrm{d}r, \qquad (2.109e)$$

Substituting (2.106) into (2.109d), we obtain

$$\mathbf{C} = -\int hg\frac{\partial r\psi}{\partial r}\, \mathrm{d}r. \qquad (2.110)$$

After integrating by parts, (2.110) becomes

$$\mathbf{C} = \int \psi g\frac{\partial h}{\partial r}\, r\mathrm{d}r. \qquad (2.111)$$

Now we define a quantity χ which satisfies

$$\mathbf{L}\chi = g\frac{\partial h}{\partial r}, \qquad (2.112)$$

with the same boundary condition as (2.107a). Substituting (2.112) into (2.110) and applying self-adjoint property, we obtain

$$\mathbf{C} = \int \psi\mathbf{L}\chi\, r\mathrm{d}r = \int \chi\mathbf{L}\psi\, r\mathrm{d}r. \qquad (2.113)$$

Substituting (2.107a) into (2.113) and integrating by parts again, we get

$$\begin{aligned}\mathbf{C} &= \int \chi\left(\frac{2mF}{gr^2} + \frac{\partial Q}{\partial r}\right)\, r\mathrm{d}r \\ &= \int Q\eta_H\, hr\mathrm{d}r + \int Fv\eta_M\, hr\mathrm{d}r, \end{aligned} \qquad (2.114)$$

where

$$\eta_H = -\frac{1}{h}\frac{\partial \chi}{\partial r}, \qquad \text{(2.115a)} \qquad\qquad \eta_M = -\frac{2m\chi}{ghvr^2}. \qquad \text{(2.115b)}$$

We refer to η_H as *dynamic efficiency of heat*, and η_M as *dynamic efficiency of momentum* which represent the conversion efficiency from potential to kinetic energy due to heating and momentum source.

Concluding Remarks

(2.107a) is different from Eliassen-Sawyer circulation equation, but it shows the similar idea; inertial stability controls the response of the system to source and sink. Indeed, if C is constant, then this is a second-order differential equation whose homogeneous solution is modified Bessel equation

$$r^2\frac{\mathrm{d}^2\psi}{\mathrm{d}r^2} + r\frac{\mathrm{d}\psi}{\mathrm{d}r} - \psi\left(1 + Cr^2\right) = r^2\frac{\partial Q}{\partial r} - \frac{2mF}{g}, \qquad \text{(2.116)}$$

where $\sqrt{C}^{-1}$ is the Rossby length of this balanced system.

CHAPTER 3
NUMERICAL METHOD

Although Eliassen-Sawyer circulation equations in different frameworks have different coefficients and geometry factors, they can still be rewritten as a general form as

$$\mathbf{L}\psi = F, \tag{3.1}$$

where

$$\mathbf{L}\left(\,\cdot\,\right) = \frac{\partial}{\partial x}\left(A\frac{\partial\left(\,\cdot\,\right)}{\partial x} + B\frac{\partial\left(\,\cdot\,\right)}{\partial y}\right) + \frac{\partial}{\partial y}\left(B\frac{\partial\left(\,\cdot\,\right)}{\partial x} + C\frac{\partial\left(\,\cdot\,\right)}{\partial y}\right). \tag{3.2}$$

Table (1) tells us how to replace x, y, A, B, and C in (3.1) to morph into different equations. (3.1) is solved by relaxation method in this study.

Derivative along x and y directions at grid point (i, j) are discretized as

$$\frac{\partial\left(\,\cdot\,\right)}{\partial x} = \frac{\left(\,\cdot\,\right)_{i+1/2,j} - \left(\,\cdot\,\right)_{i-1/2,j}}{\Delta x}, \tag{3.3a}$$

$$\frac{\partial\left(\,\cdot\,\right)}{\partial y} = \frac{\left(\,\cdot\,\right)_{i,j+1/2} - \left(\,\cdot\,\right)_{i,j-1/2}}{\Delta y}, \tag{3.3b}$$

where Δx and Δy are grid spacings.

Table 1: General form of Eliassen-Sawyer circulation equation in different coordinates

Variables in (3.1)	Quasi-geostrophic	Cartesian	Cylindrical	Spherical
x	y	y	r	$a\phi$
y	z	z	z	z
ψ	ψ	ψ	$r\psi$	$R\psi$
A	A	A	A/r	A/R
B	0	B	B/r	B/R
C	C	C	C/r	C/R

After applying (3.3) to (3.1) at grid point (i,j) ($2 \le i \le n_x - 1$ and $2 \le i \le n_x - 1$),

$$\begin{aligned}\frac{\partial}{\partial x}\left(A\frac{\partial \psi}{\partial x}\right) &= \frac{1}{\Delta x}\left[A_{i+1/2,j}\left(\frac{\partial \psi}{\partial x}\right)_{i+1/2,j} - A_{i-1/2,j}\left(\frac{\partial \psi}{\partial x}\right)_{i-1/2,j}\right] \\ &= \frac{1}{(\Delta x)^2}\left[A_{i+1/2,j}(\psi_{i+1,j} - \psi_{i,j}) - A_{i-1/2,j}(\psi_{i,j} - \psi_{i-1,j})\right] \\ &= \frac{1}{(\Delta x)^2}\left[\psi_{i+1,j}A_{i+1/2,j} + \psi_{i-1,j}A_{i-1/2,j} - \psi_{i,j}(A_{i-1/2,j} + A_{i+1/2,j})\right], \end{aligned} \tag{3.4a}$$

$$\frac{\partial}{\partial y}\left(C\frac{\partial \psi}{\partial y}\right) = \frac{1}{(\Delta y)^2}\left[\psi_{i,j+1}C_{i,j+1/2} + \psi_{i,j-1}C_{i,j-1/2} - \psi_{i,j}(C_{i,j-1/2} + C_{i,j+1/2})\right], \tag{3.4b}$$

$$\begin{aligned}\frac{\partial}{\partial x}\left(B\frac{\partial \psi}{\partial y}\right) = \frac{1}{\Delta x \Delta y}\big[&B_{i+1/2,j}(\psi_{i+1/2,j+1/2} - \psi_{i+1/2,j-1/2}) \\ &- B_{i-1/2,j}(\psi_{i-1/2,j+1/2} - \psi_{i-1/2,j-1/2})\big], \end{aligned} \tag{3.4c}$$

$$\begin{aligned}\frac{\partial}{\partial y}\left(B\frac{\partial \psi}{\partial x}\right) = \frac{1}{\Delta x \Delta y}\big[&B_{i,j+1/2}(\psi_{i+1/2,j+1/2} - \psi_{i-1/2,j+1/2}) \\ &- B_{i,j-1/2}(\psi_{i+1/2,j-1/2} - \psi_{i-1/2,j-1/2})\big]. \end{aligned} \tag{3.4d}$$

We define

$$\psi_{i+1/2,j+1/2} = \frac{1}{2}\left(\psi_{i+1,j} + \psi_{i,j+1}\right), \tag{3.5a}$$

$$\psi_{i-1/2,j+1/2} = \frac{1}{2}\left(\psi_{i-1,j} + \psi_{i,j+1}\right), \tag{3.5b}$$

$$\psi_{i+1/2,j-1/2} = \frac{1}{2}\left(\psi_{i+1,j} + \psi_{i,j-1}\right), \tag{3.5c}$$

$$\psi_{i-1/2,j-1/2} = \frac{1}{2}\left(\psi_{i-1,j} + \psi_{i,j-1}\right), \tag{3.5d}$$

to rewrite (3.4c) as

$$\begin{aligned}&\frac{\partial}{\partial x}\left(B\frac{\partial \psi}{\partial y}\right) + \frac{\partial}{\partial y}\left(B\frac{\partial \psi}{\partial x}\right) \\ &\quad= \frac{1}{2\Delta x \Delta y}\left[\psi_{i+1,j}\left(B_{i,j+1/2} - B_{i,j-1/2}\right) + \psi_{i-1,j}\left(B_{i,j-1/2} - B_{i,j+1/2}\right)\right. \\ &\qquad\left. + \psi_{i,j+1}\left(B_{i+1/2,j} - B_{i-1/2,j}\right) + \psi_{i,j-1}\left(B_{i-1/2,j} - B_{i+1/2,j}\right)\right]. \end{aligned} \tag{3.6}$$

Finally, (3.1) becomes

$$\frac{\partial}{\partial x}\left(A\frac{\partial \psi}{\partial x}+B\frac{\partial \psi}{\partial y}\right)+\frac{\partial}{\partial y}\left(B\frac{\partial \psi}{\partial x}+C\frac{\partial \psi}{\partial y}\right)=\boldsymbol{M}^{\mathrm{T}}\boldsymbol{\Psi}-S\psi_{i,j}, \tag{3.7}$$

where

$$\boldsymbol{M}=\begin{bmatrix} \frac{C_{i,j-1/2}}{(\Delta y)^2}+\frac{B_{i-1/2,j}-B_{i+1/2,j}}{2\Delta x\Delta y} \\ \frac{A_{i-1/2,j}}{(\Delta x)^2}+\frac{B_{i-1/2,j}-B_{i+1/2,j}}{2\Delta x\Delta y} \\ \frac{A_{i+1/2,j}}{(\Delta x)^2}+\frac{B_{i,j+1/2}-B_{i,j-1/2}}{2\Delta x\Delta y} \\ \frac{C_{i,j+1/2}}{(\Delta y)^2}+\frac{B_{i+1/2,j}-B_{i-1/2,j}}{2\Delta x\Delta y} \end{bmatrix}, \tag{3.8a}$$

$$\boldsymbol{\Psi}=\begin{bmatrix} \psi_{i,j-1} \\ \psi_{i-1,j} \\ \psi_{i+1,j} \\ \psi_{i,j+1} \end{bmatrix}, \tag{3.8b}$$

are two column matrix, and

$$S=\frac{A_{i-1/2,j}+A_{i+1/2,j}}{(\Delta x)^2}+\frac{C_{i,j-1/2}+C_{i,j+1/2}}{(\Delta y)^2}. \tag{3.8c}$$

We define iteration from n to $n+1$ to be

$$\psi_{i,j}^{n+1}=\psi_{i,j}^{n}+\frac{\mathfrak{R}}{S}, \tag{3.9}$$

where

$$\mathfrak{R}=\boldsymbol{M}^{\mathrm{T}}\boldsymbol{\Psi}^{n}-S\psi_{i,j}^{n}-\boldsymbol{F}, \tag{3.10}$$

and **F** is the matrix form of F in (3.1). To estimate the error, substitute (3.10) into (3.9) to get

$$\boldsymbol{M}^{\mathrm{T}}\boldsymbol{\Psi}^{n}-S\psi_{i,j}^{n+1}=\boldsymbol{F}. \tag{3.11}$$

Suppose there exists exact solution ψ^* such that

$$\boldsymbol{M}^{\mathrm{T}}\boldsymbol{\Psi}^{*}-S\psi_{i,j}^{*}=\boldsymbol{F}, \tag{3.12}$$

where asterisk superscript denotes exact solution. Extract (3.12) from (3.11) and define

error at the nth iteration time at grid point (i,j) as $\mathfrak{E}^n_{i,j} = \psi^n_{i,j} - \psi^*_{i,j}$ then we have

$$\boldsymbol{M}^{\mathrm{T}}\boldsymbol{E}^n - S\mathfrak{E}^{n+1}_{i,j} = 0, \tag{3.13}$$

where

$$\boldsymbol{E}^n = \begin{bmatrix} \mathfrak{E}_{i,j-1} \\ \mathfrak{E}_{i-1,j} \\ \mathfrak{E}_{i+1,j} \\ \mathfrak{E}_{i,j+1} \end{bmatrix}. \tag{3.14}$$

Solving $\mathfrak{E}^{n+1}_{i,j}$, we get

$$\mathfrak{E}^{n+1}_{i,j} = \frac{1}{S}\boldsymbol{M}^{\mathrm{T}}\mathfrak{E}^n. \tag{3.15}$$

If $A, C > 0$ and B is relatively small, then the error at $(n+1)$th time is the average of its adjacent error at nth time because the sum of elements in $\boldsymbol{M}$ is exactly S. (3.15) converges to zero if error on boundary is zero, implying $\psi^n \to \psi^*$.

To measure the average error, the average residual of the nth iteration is defined as

$$\mathfrak{E}^n_{\text{avg}} = \sqrt{\frac{1}{N}\sum_{i,j}\left(\mathfrak{E}^n_{i,j}\right)^2}, \tag{3.16}$$

where N is the number of grid points.

When to stop iteration needs convergence criteria. In our program we use both the magnitude of residual, relative convergence speed and convergence counter to ensure our solution approximates true solution. To be clear, the iteration stops at the nth and gives no warning/error if and only if

1. $\mathfrak{E}^n_{\text{avg}} \leq \mathfrak{E}_{\text{max}}$
2. $\left|\frac{\mathfrak{E}^n_{\text{avg}} - \mathfrak{E}^{n-1}_{\text{avg}}}{\mathfrak{E}^{n-1}_{\text{avg}}}\right| \leq \mathfrak{O}_{\text{max}}$
3. $n \leq n_{\text{max}}$

(3.8a) can be calculated beforehand to reduce computation time.

The grid point used in this method is arrange as Fig. 1.

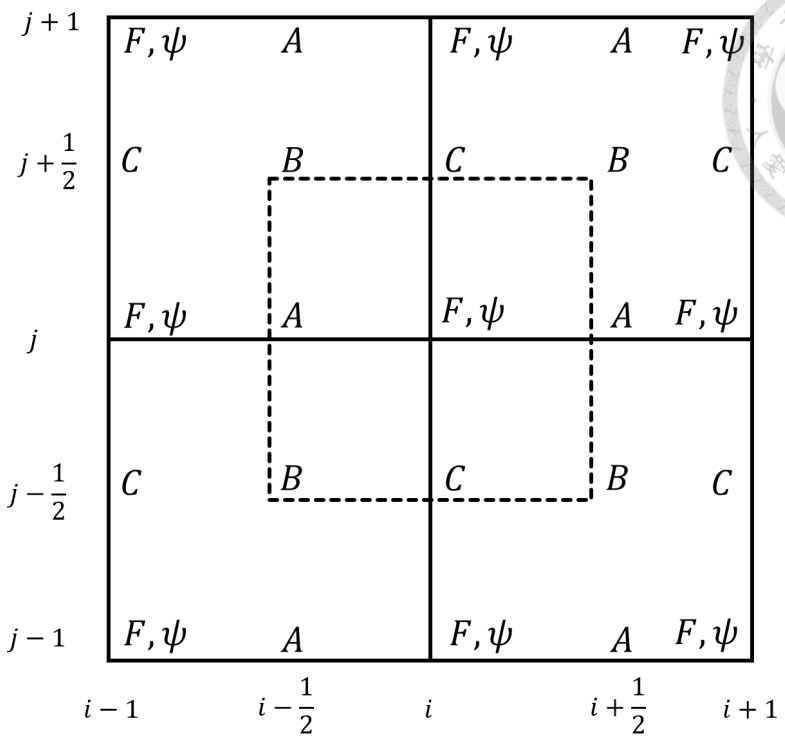

Figure 1: Finite-difference grid for solutions of (3.1)

The API for relaxation method is shown in appendix E. The code is written in Fortran 95 and maintained on Github (`http://github.com/meteorologytoday/XLab-EE-fortran`).

CHAPTER 4
NUMERICAL EXPERIMENTS

General interaction between heating and its response is schematically shown in Fig. 2. It shows that the heating is a forcing, but also can be adjust by feedback from dynamics of the system. Our numerical experiments focus on the upper part, i.e. how the heating generate its dynamic response.

The diagnose procedure is shown in Sec. 4.1. The numerical settings for vortex and heating are shown in Sec. 4.2. Results for single eyewall are in Sec. 4.3. Results for concentric eyewall are in Sec. 4.4. Results for structure test and sensitivity test are in Sec. 4.5-4.9

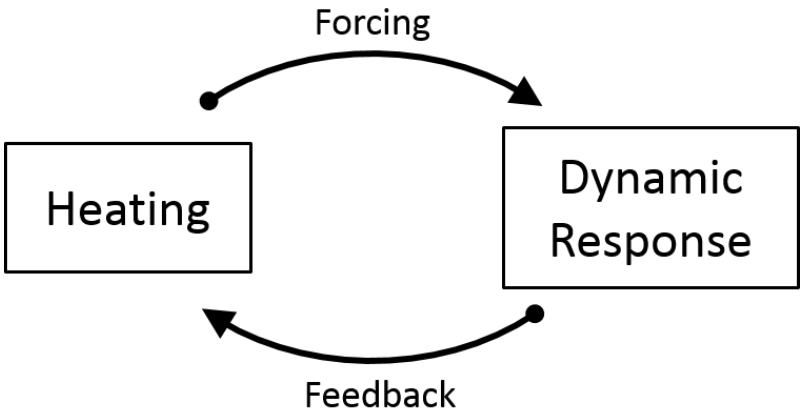

Figure 2: General scheme of a tropical cyclone system. Heating is treated as a forcing to generate dynamic response which feedbacks to heating at the same time. Our work is to diagnose the effect of the heating and to discuss its dynamic response.

4.1 Diagnose Procedure

To see the response of heating inside a cyclone, we need secondary circulation (2.64), Eliassen-Sawyer circulation equation (2.65a), thermodynamic equation (2.59e), equation (2.70) for χ and equation (2.73) for dynamic efficiency. The diagnose procedure is as follows:

1. Specify A, B, C, Q, F.
2. Invert ψ by Eliassen-Sawyer circulation equation (2.65a) with Jacobi relaxation method (chapter 3). Specify boundary condition if needed.
3. Calculate secondary circulation by (2.64).
4. Calculate $\dfrac{\partial\theta}{\partial t}$ by thermodynamic equation (2.59e).
5. Calculate $\theta_{new} = \theta_{old} + \dfrac{\partial\theta}{\partial t}\Delta t$.
6. Invert χ by equation (2.70) with Jacobi relaxation method. $r\chi \to 0$ on boundary.
7. Calculate dynamic efficiency η_H, η_M with equation (2.73).

4.2 Vortex and Heating Settings

All simulations in this paper differ in number of regions.

For all cases, the following variables are the same:

$$A = N^2 \tag{4.1a}$$

$$B = 0 \tag{4.1b}$$

$$F = 0 \tag{4.1c}$$

The vortex is divided into n regions by $n-1$ radius $\left\{ r_k \middle| 1 \le k \le n-1 \right\}$. The heating Q is defined as a half-sined shape confined between z_B and z_T in height

$$Q\left(r,z\right) = \hat{Q}\left(r\right) \sin\left(\pi \frac{z - z_B}{z_T - z_B}\right) \tag{4.2}$$

where

$$\hat{Q}\left(r\right) = \begin{cases} \hat{Q}_1 & \text{if} \quad r < r_1 \\ \hat{Q}_k & \text{if} \quad r_k - 1 \le r < r_k \text{ for } k = 2, 3, ..., n-2 \\ 0 & \text{if} \quad r \ge r_{n-1} \end{cases} \tag{4.3}$$

and total integral of Q is conserved

$$\int_0^\infty \hat{Q}\ \mathrm{d}r^2 = \hat{Q}_1 r_1^2 + \sum_{k=2}^{n-1} \hat{Q}_k \left(r_k^2 - r_{k-1}^2\right) = \mathbf{H_0} \tag{4.4}$$

Inertial stability C is defined as

$$C = \hat{f}^2\left(r\right) \tag{4.5}$$

where

$$\hat{f}\left(r\right) = \begin{cases} \hat{f}_1 & \text{if} \quad r < r_1 \\ \hat{f}_k & \text{if} \quad r_{k-1} \le r < r_k \text{ for } k = 2, 3, ..., n-2 \\ \hat{f}_n & \text{if} \quad r \ge r_{n-1} \end{cases} \tag{4.6}$$

Inverse of Rossby length is defined as

$$\hat{\mu}\left(r\right) = \frac{\hat{f}\left(r\right)}{N\left(z_\infty - z_0\right)} \tag{4.7}$$

Similar to (4.6), distribution of μ in (4.7) is

$$\hat{\mu}(r) = \begin{cases} \hat{\mu}_1 & \text{if} \quad r < r_1 \\ \hat{\mu}_k & \text{if} \quad r_{k-1} \leq r < r_k \text{ for } k = 2, 3, ..., n-2 \\ \hat{\mu}_n & \text{if} \quad r \geq r_{n-1} \end{cases} \tag{4.8}$$

where

$$\hat{\mu}_k = \frac{\hat{f}_k}{N(z_\infty - z_0)} \tag{4.9}$$

For constants, we take $N = 1.2 \times 10^{-2}\text{s}^{-1}$, $f = 5 \times 10^{-5}\text{s}^{-1}$, $\mu = 1000\text{km}$, $g = 9.8\text{m s}^{-2}$.

For all cases, domain width and height are 1000km and $c_p\theta_0/g \approx 30$km . We use 51 points in z direction, 1001 points in r direction. $z_T = z_\infty$ and $z_B = z_0$ in all cases if not mentioned.

The setting details are listed in Table 2-4.

4.3 Single eyewall cyclone

The first set of experiments is to examine single eyewall cyclone. The result is shown in Fig 3. The efficiency plot (f) reveals the connection to temperature anomaly (c): the contour of them are very similar, and the overlap of heating region and peak of efficiency supports the idea stating that heating intensifies the vortex. Notice that this calculation is under Boussinesq approximation which is equivalent using constant density so that the contour is vertically symmetric.

We also apply this to five stages of typical development of tropical cyclone, the result is shown in Fig 4. The average efficiency of heat grows as cyclone intensifies. These data are adapted from Schubert and Hack (1982) in which they construct these curves so as to be consistent with the observational results of Shea and Gray (1973) and Holliday and Thompson (1979).

We also plot the local heating response and average efficiency of heat in terms of the eye strength and the size of eye (Fig 5). Notice the development of a typical cyclone from A to E. One explanation is that in the initial stage A, vortex is not easy to accumulate

Table 2: Two-regioned model settings for typical development of tropical cyclone. $\mathbf{H_0} = 10$ K day^{-1} $(250\text{km})^2$

Case	r_1 [km]	δ_1	$\hat{Q}_1$ [K day^{-1}]
A	300	0	6.94
B	250	2	10.00
C	200	4	15.63
D	150	10	27.78
E	100	24	62.50

Table 3: Three-regioned model settings for u-shaped wind profile. $\mathbf{H_0} = 125$ K day^{-1} $(50\text{km})^2$

Case	(r_1, r_2) [km]	(δ_1, δ_2)	$\hat{Q}_2$ [K hr^{-1}]
A	$(10, 20)$	$(140.0, 140.0)$	43.4
B	$(10, 20)$	$(40.0, 144.2)$	43.4
C	$(30, 40)$	$(70.0, 70.0)$	18.6
D	$(30, 40)$	$(13.3, 84.3)$	18.6

Table 4: Five-regioned model settings for decoupled wind and heating profile. $\mathbf{H_0} = 125$ K day^{-1} $(50\text{km})^2$

Case	(r_1, r_2, r_3, r_4) [km]	$(\hat{\mu}_1, \hat{\mu}_2, \hat{\mu}_3, \hat{\mu}_4)$ [km]	$\left(\hat{Q}_2, \hat{Q}_4\right)$ [K hr^{-1}]
A_{dyn}	$(8, 15, 79, 85)$	$(5.5, 8.5, 1000, 1000)$	-
A_{heat}	$(8, 15, 79, 85)$	-	$(21.5, 9.71)$
B_{dyn}	$(8, 15, 56, 62)$	$(5.5, 8.5, 72.8, 36.5)$	-
B_{heat}	$(8, 15, 56, 62)$	-	$(21.5, 13.5)$
C_{dyn}	$(8, 15, 79, 85)$	$(5.5, 8.5, 27.2, 14.9)$	-
C_{heat}	$(8, 15, 34, 40)$	-	$(21.5, 21.5)$
Heating $2:1$	$(8, 15, 34, 40)$	-	$(34.0, 17.0)$
Heating $1:1$			$(21.5, 21.5)$
Heating $1:2$			$(12.4, 24.8)$

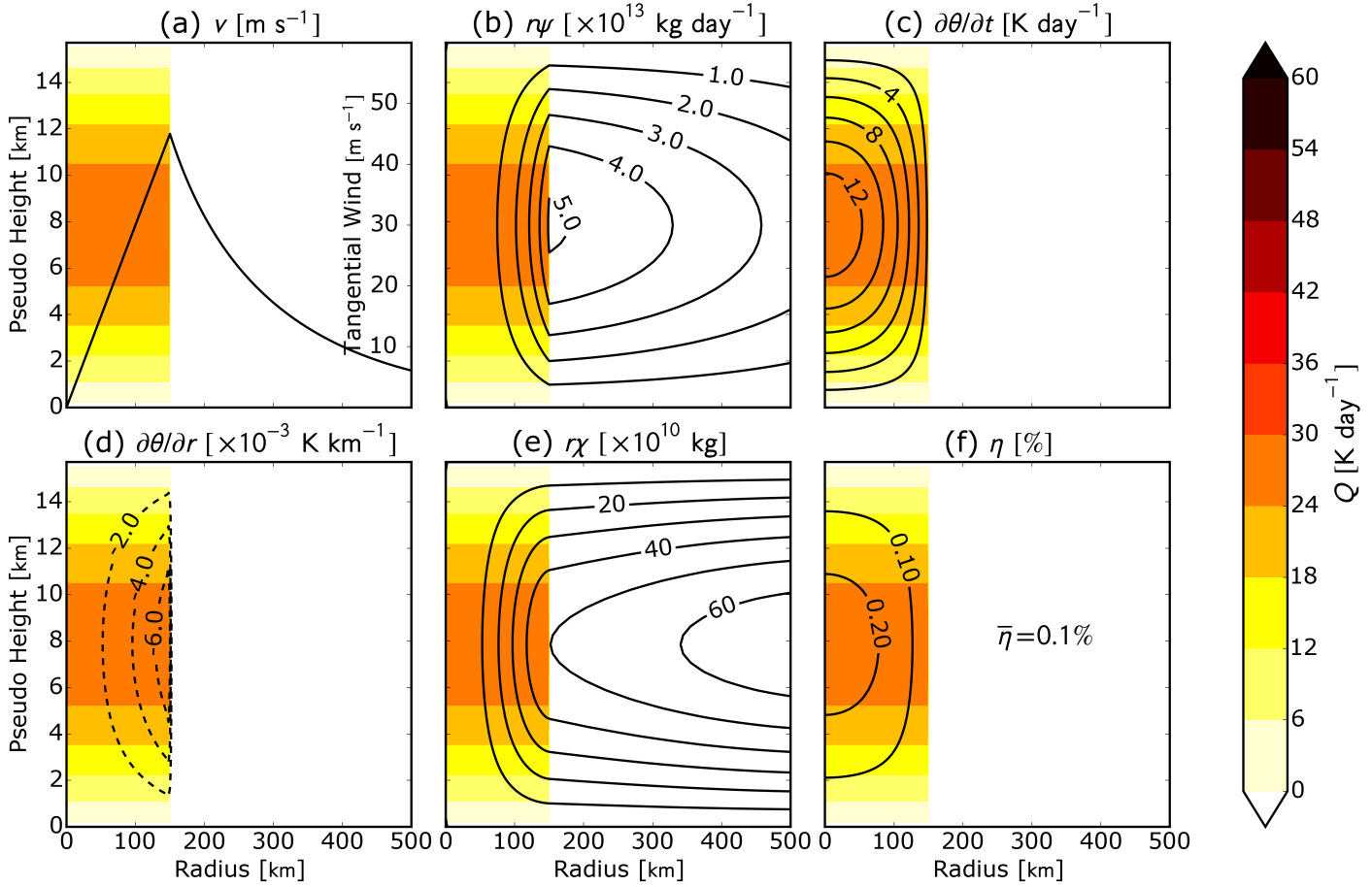

Figure 3: The flowchart of a two-regioned barotropic model which represents a single eyewall tropical cyclone. (a) Tangential wind profile (m s^{-1}). (b) Induced streamfunction $r\psi$ ($\times 10^{13}$ kg day^{-1}). (c) Local heating rate $\partial T/\partial t$ (K day^{-1}). (d) $\partial T/\partial r$ ($\times 10^{-3}$ K km^{-1}). Time interval is one hour. (e) Corresponding solution $r\chi$ ($\times 10^{10}$ kg). (f) Dynamic efficiency of heat (%). Shades in all graphs are adiabatic heating (K day^{-1}). The model setting is adapted from Schubert and Hack (1982) and is listed in table 2 (case D).

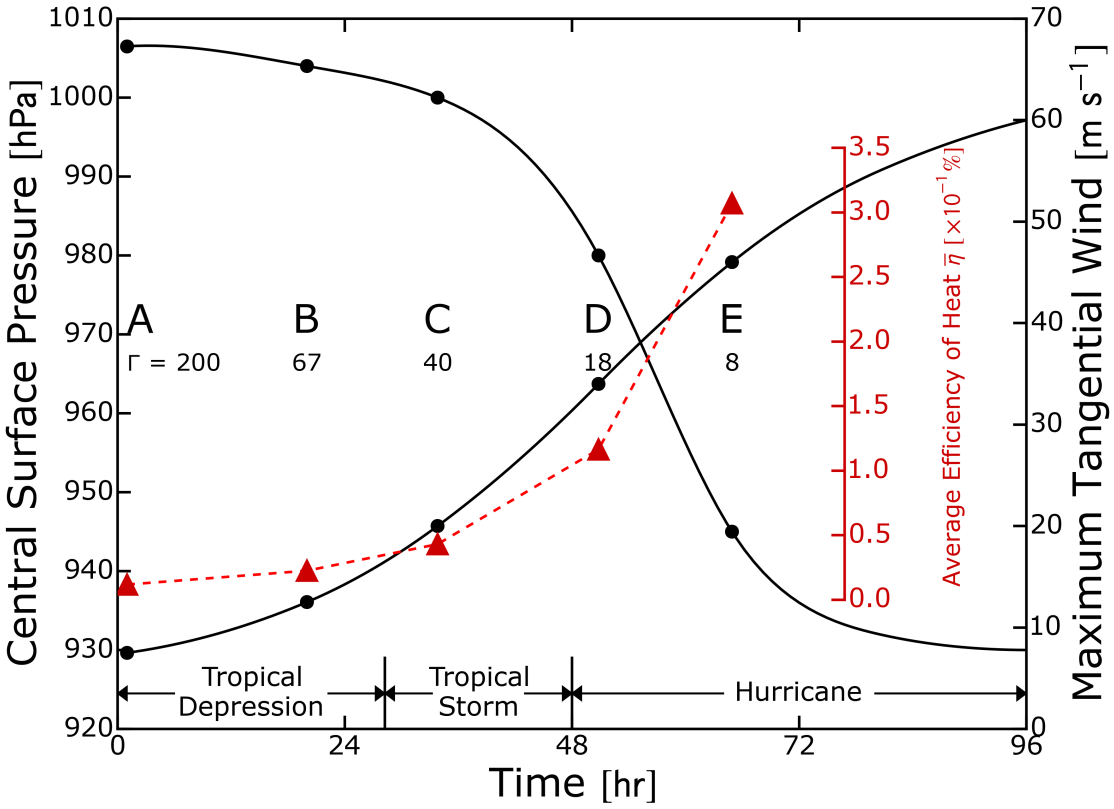

Figure 4: Evolution with repect to total time (hr) of average efficiency of heat $\overline{\eta}$ ($\times 10^{-1}$%, red line), maximum wind speed (m s^{-1}), $\Gamma = \sqrt{A/C}$ (labeled under each stage) and central pressure (hpa) of five stages during a typical tropical cyclone development. Time interval is one hour. The model settings are adapted from Schubert and Hack (1982) and are listed in table 2.

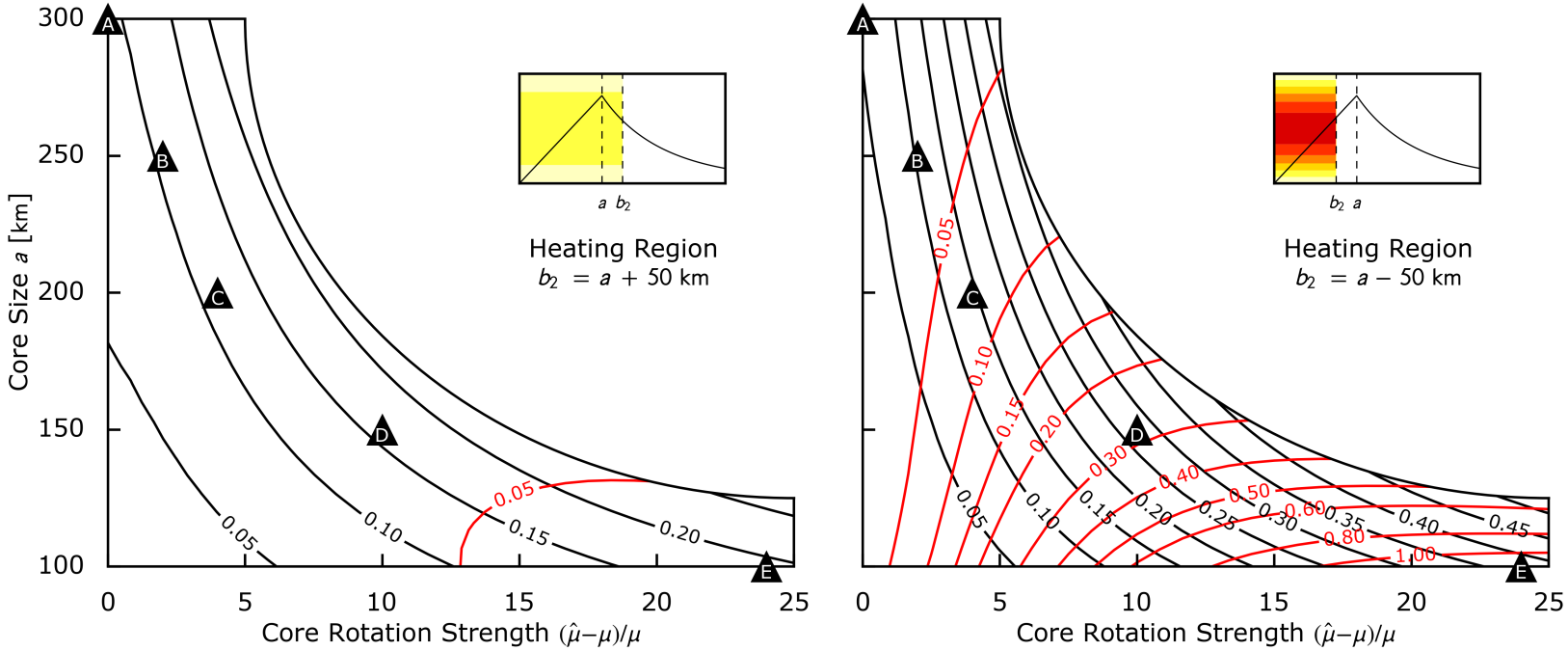

Figure 5: Isolines of total heat response ($\int_0^{b_2} \frac{\partial T}{\partial t} r dr / \int_0^{b_2} Q r dr$, black line) and average efficiency $\overline{\eta}$ (%, red line) in terms of core size a (km) and core rotation strength $(\hat{\mu} - \mu)/\mu$ with different heating region $b_2 = a \pm 50$km. A, B, C, D and E represent five stages of typical tropical cyclone. The model settings are the same as Fig. 4

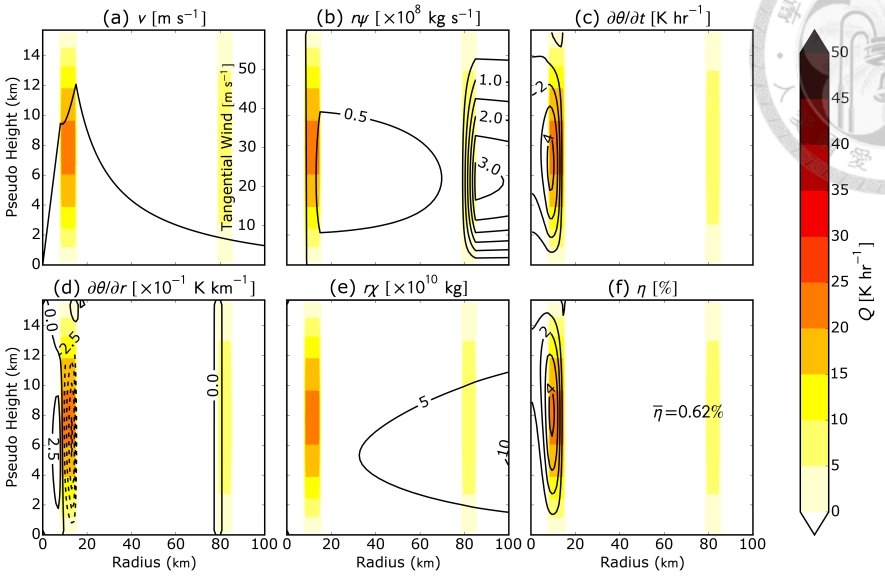

Figure 6: The flowchart of a five-regioned barotropic model which represents a double eyewall tropical cyclone. (a) Tangential wind profile ($\mathrm{m\,s^{-1}}$). (b) Induced streamfunction $r\psi$ ($\times 10^8$ kg $\mathrm{s^{-1}}$). (c) Local heating rate $\partial T/\partial t$ (K $\mathrm{hr^{-1}}$). (d) $\partial T/\partial r$ ($\times 10^{-1}$ K $\mathrm{km^{-1}}$). Time interval is one hour. (e) Corresponding solution $r\chi$ ($\times 10^{10}$ kg). (f) Dynamic efficiency of heat (%). Shades in all graphs are adiabatic heating ($\mathrm{K\,day^{-1}}$). The model setting is adapted from Rozoff et al. (2008) and listed in table 4 (case $\mathrm{A_{dyn} + A_{heat}}$).

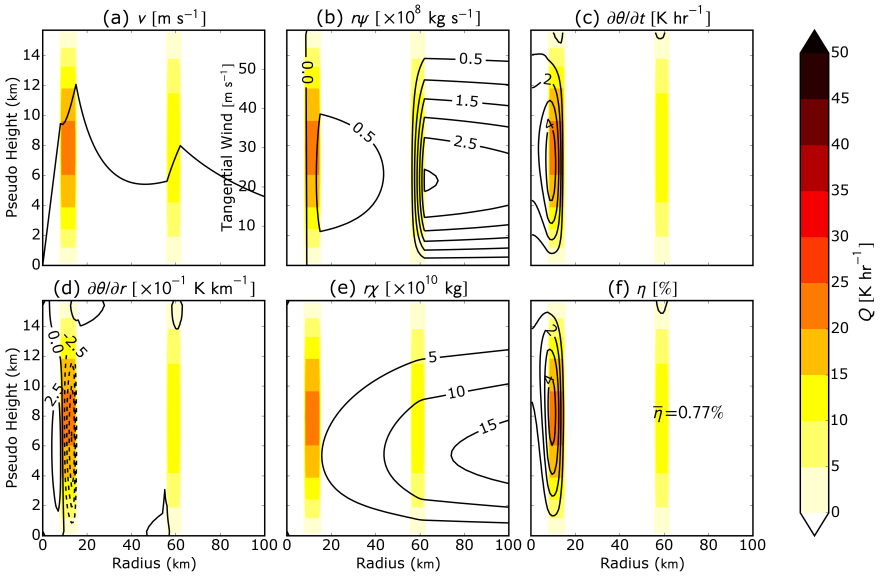

Figure 7: The flowchart of a five-regioned barotropic model which represents a double eyewall tropical cyclone. (a) Tangential wind profile ($\mathrm{m\,s^{-1}}$). (b) Induced streamfunction $r\psi$ ($\times 10^8$ kg $\mathrm{s^{-1}}$). (c) Local heating rate $\partial T/\partial t$ (K $\mathrm{hr^{-1}}$). (d) $\partial T/\partial r$ ($\times 10^{-1}$ K $\mathrm{km^{-1}}$). Time interval is one hour. (e) Corresponding solution $r\chi$ ($\times 10^{10}$ kg). (f) Dynamic efficiency of heat (%). Shades in all graphs are adiabatic heating ($\mathrm{K\,day^{-1}}$). The model setting is adapted from Rozoff et al. (2008) and listed in table 4 (case $\mathrm{B_{dyn} + B_{heat}}$).

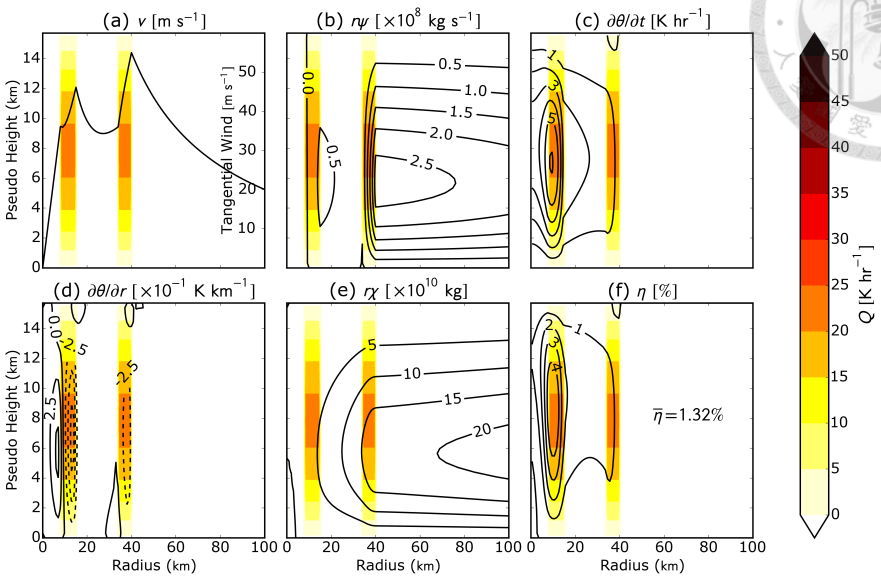

Figure 8: The flowchart of a five-regioned barotropic model which represents a double eyewall tropical cyclone. (a) Tangential wind profile ($\mathrm{m\,s^{-1}}$). (b) Induced streamfunction $r\psi$ ($\times 10^8$ kg $\mathrm{s^{-1}}$). (c) Local heating rate $\partial T/\partial t$ (K $\mathrm{hr^{-1}}$). (d) $\partial T/\partial r$ ($\times 10^{-1}$ K $\mathrm{km^{-1}}$). Time interval is one hour. (e) Corresponding solution $r\chi$ ($\times 10^{10}$ kg). (f) Dynamic efficiency of heat (%). Shades in all graphs are adiabatic heating ($\mathrm{K\,day^{-1}}$). The model setting is adapted from Rozoff et al. (2008) and listed in table 4 (case $\mathrm{C_{dyn}} + \mathrm{C_{heat}}$).

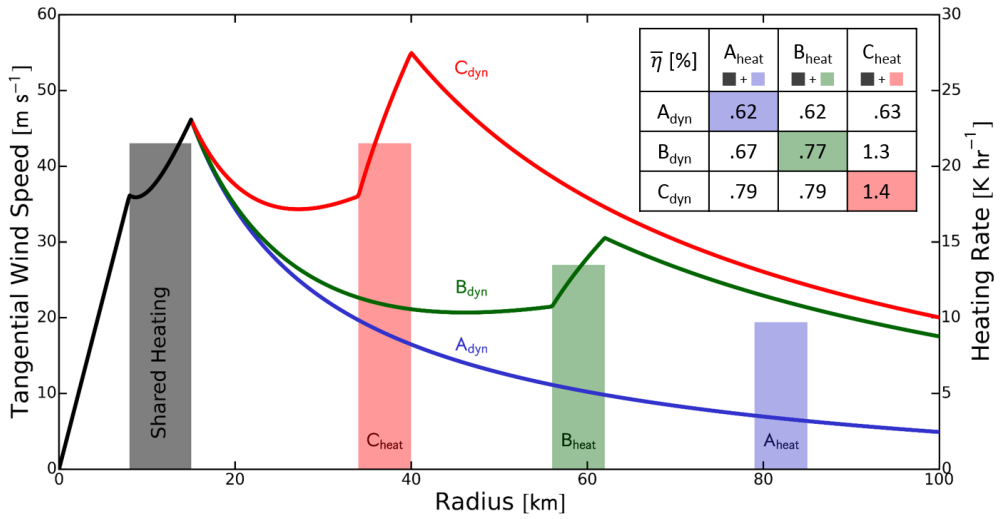

Figure 9: Three settings of tangential wind speed profile (m $\mathrm{s^{-1}}$, solid lines) and heat constant $\hat{Q}$ (K $\mathrm{hr^{-1}}$). The coupled results of average efficiency $\overline{\eta}$ (%) are listed in the top-right table. Time interval is one hour. The model settings are adapted from Rozoff et al. (2008) and are listed in table 4.

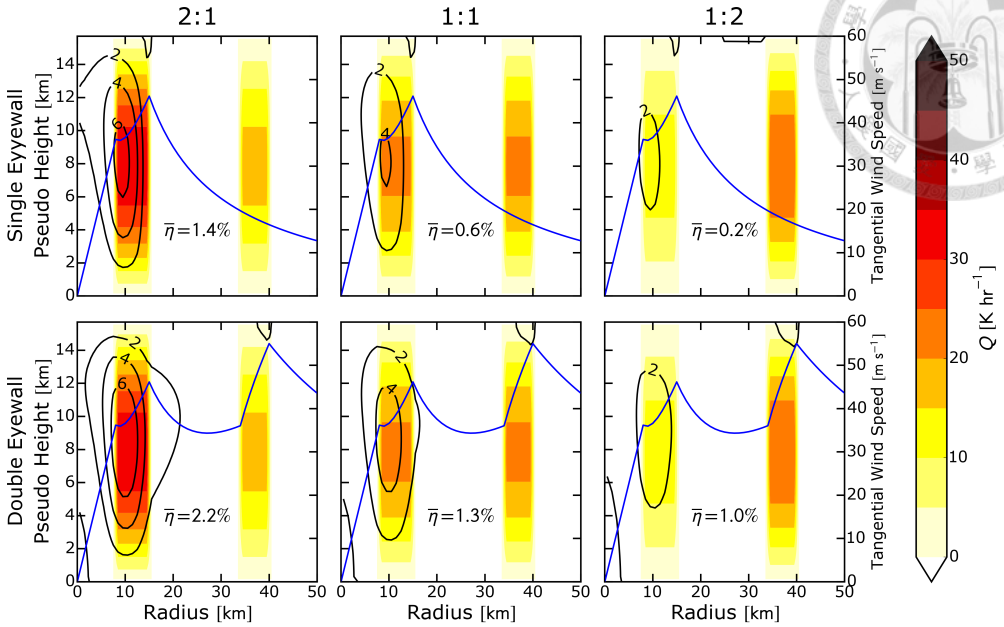

Figure 10: The wind profile (m s^{-1}, solid line), heating (K hr^{-1}, shading) and result efficiency η ($\times 10^{-1}$%, contour) of six different cases. The wind profiles represent single (A_{dyn}) and double (C_{dyn}) eyewall and in the first and second rows, respectively. The heating ratios between inner and outer eyewalls are $2:1$, $1:1$ and $1:2$ (shown in table 4) in the first, second and third columns, respectively.

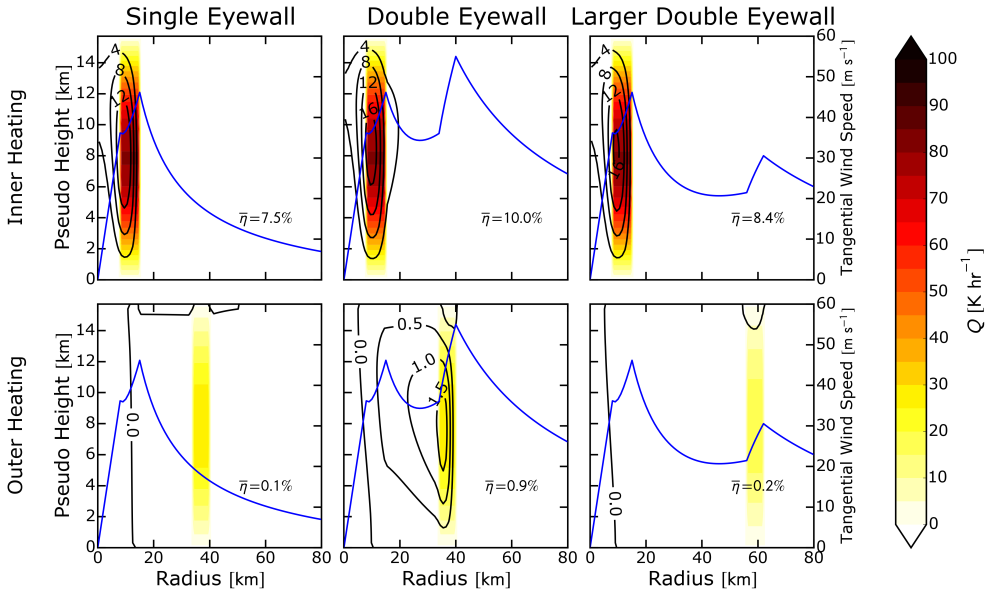

Figure 11: The wind profile (m s^{-1}, solid line), heating (K hr^{-1}, shading) and result efficiency η ($\times 10^{-1}$%, contour) of six different cases. The wind profiles represent single, double, and larger double eyewall (A_{dyn}, B_{dyn} and C_{dyn}) in the first, second and third columns, respectively. The heating is totally on inner eyewall and outer eyewall (80.9, 29.3 and 18.4 K hr^{-1}) in the first and second rows, respectively.

potential energy and to release it into kinetic energy because of low local heating response and efficiency of heat while in the final stage E it is easy to accumulate potential energy and to release it into kinetic energy because of high local heating response and efficiency of heat.

4.4 Concentric eyewall cyclone

We see that in Fig. 6-8 there are two efficiency peaks emerging. Each peak corresponds to a heating maximum but the inner one is much more efficient than the outside.

To see the effect of inner/outer eyewall, we adapt the setting from Rozoff et al. (2008). By decoupling the heating and wind fields, Fig. 9 shows that a concentric eyewall cyclone tends to get high response of efficiency when heating is inside the eye and when outer eyewall is small and strong (i.e. high inertial stability). However, outer eyewall position in this experiment is not fixed, so it remains unclear what role does outer eyewall plays.

Now we design an experiment with the position of outer eyewall fixed by using wind profile A and C above as single and double eyewall. Moreover, we also alter the heating ratio between inner and outer eyewall (Fig. 10). When turning on the outer eyewall (second row), or putting more heating on the inner eyewall (first column), both the average efficiency and peak value get higher. It is because the outer eyewall (large $C = \hat{f}^2$) reduces the Rossby deformation length (also see (2.80))

$$\hat{\mu}^{-1} = \frac{N\left(z_\infty - z_0\right)}{\hat{f}\pi}, \tag{4.10}$$

so that it blocks the outflow of the air inside and makes local heating more efficient. This result is consistent with Schubert and McNoldy (2010).

In the next experiment (Fig. 11) we consider heating totally on inner/outer eyewall with different outer eyewall configuration. The first column represents single eyewall scenario. Comparing the first and second or first and third columns, it shows that the outer eyewall enhances the efficiency. Comparing the first row and second row of the second or third column, it shows that heating on inner eyewall is better than heating outside the

eyewall. Comparing second and third columns, it show that efficiency of outer eyewall of smaller radius is larger than the larger one. We use a table (table 5) to summarize the experiment results of concentric eyewall.

Table 5: Average efficiency $\overline{\eta}$ (%) with respect to heating distance $r_3 - r_2$ (km) and heating ratio $Q_2 : Q_4$ between inner and outer eyewall.

$\overline{\eta}$[%]		Heating Distance $r_3 - r_2$ [km]		
		19	41	64
Heating Ratio $Q_2 : Q_4$	100:0	10.1	8.4	7.5
	75:25	3.1	1.5	0.9
	50:50	1.3	0.4	0.2
	25:75	0.9	0.2	0.1

4.5 Eye with hub cloud

Simpson and Starrett (1955) presented the schematic reproduced aircraft data emphasizing the fact that the hurricane eye often contains low-level stratocumulus known as "hub cloud" near the circulation center, surrounded by a "moat" of clear air or thin stratocumulus near the outer edge of the eye. Schubert et al. (2007) proved this to be related to the U-shaped wind profile characterizing strong inertial stability near the eye, making the maximum downward motion located at some finite distance away from the eye.

To see if hub cloud does any difference inside a cyclone, we adapt the setting from Schubert et al. (2007) . The results are shown in Fig 12. Though the average efficiency makes small difference between hub/nonhub cloud cases, the contour of efficiency shows that their structures differ: non-hub cloud profile elongates the distribution of the efficiency of heat while the other does not. The reason they have similar average efficiency is clear: their overlapping with heating region are almost identical so that we cannot tell the difference. We conclude that efficiency structures differ in a strong inertial stability eye but average efficiencies are the same, because elongated part is not overlapped with heating region.

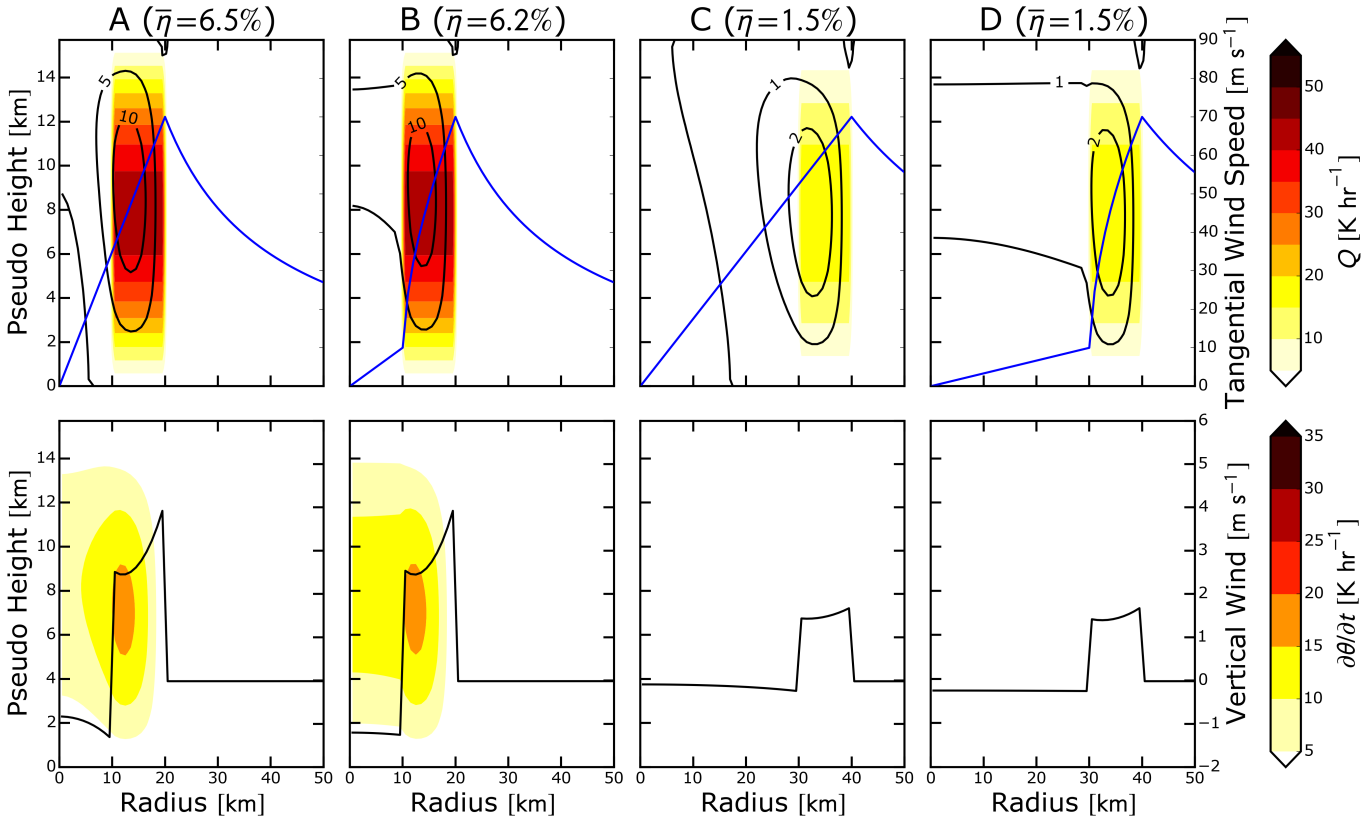

Figure 12: Four cases to compare hub-cloud profile's efficiency. The first row is wind profile, heating (K hr^{-1}, shading), and result efficiency $\overline{\eta}$ ($\times 10^{-1}$%, contour), the second row shows the induced vertical motion w (m s^{-1}) and local heating rate $\partial T/\partial t$ (K hr^{-1}). The model settings are adapted from Schubert et al. (2007) and are listed in table 3

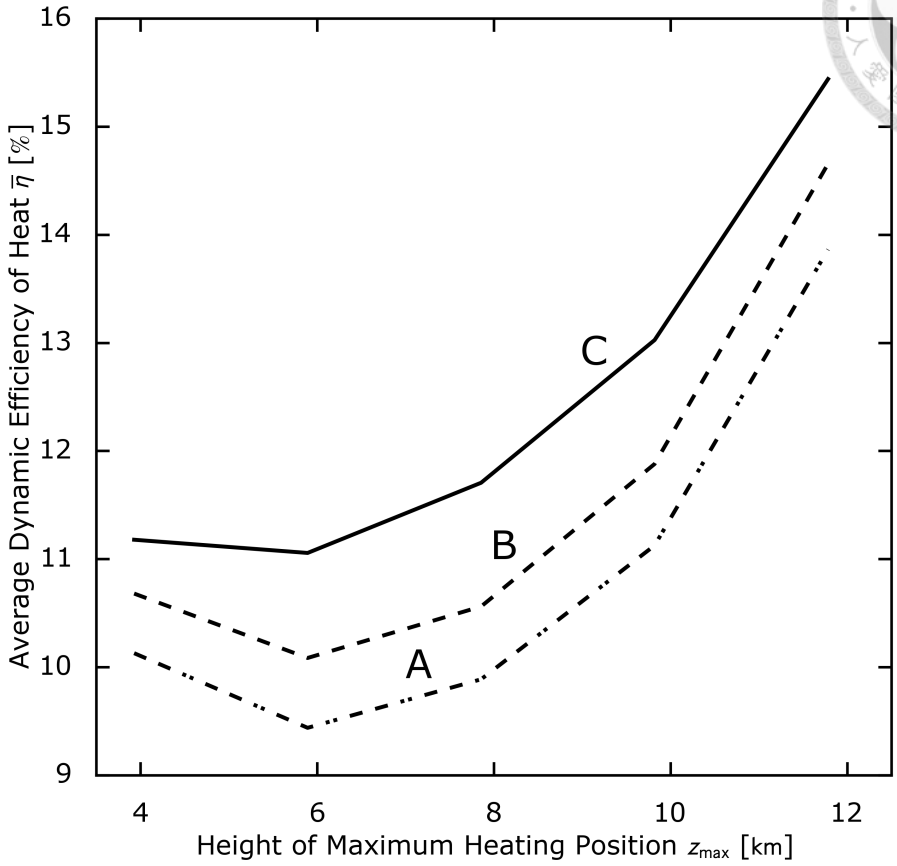

Figure 13: Average dynamic efficiency of heat $\overline{\eta}$ (%) in various height of maximum heating $z_{\max}$ (km). Heating thickness is half of the atmosphere height. A, B and C represent wind profile as in Fig. 9 Notice that heating is now totally in the first eyewall.

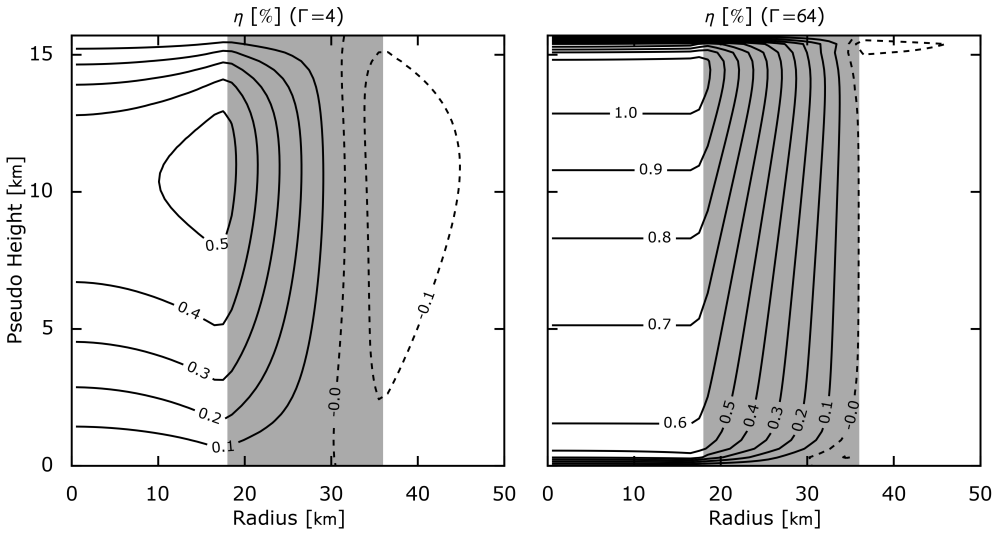

Figure 14: Distribution of dynamic efficiency of heat (%, contour) under pre-existing baroclinity (shaded) with different Γ (4 and 64). $B = 1 \times 10^{-6}\mathrm{s}^{-2}$ in both cases.

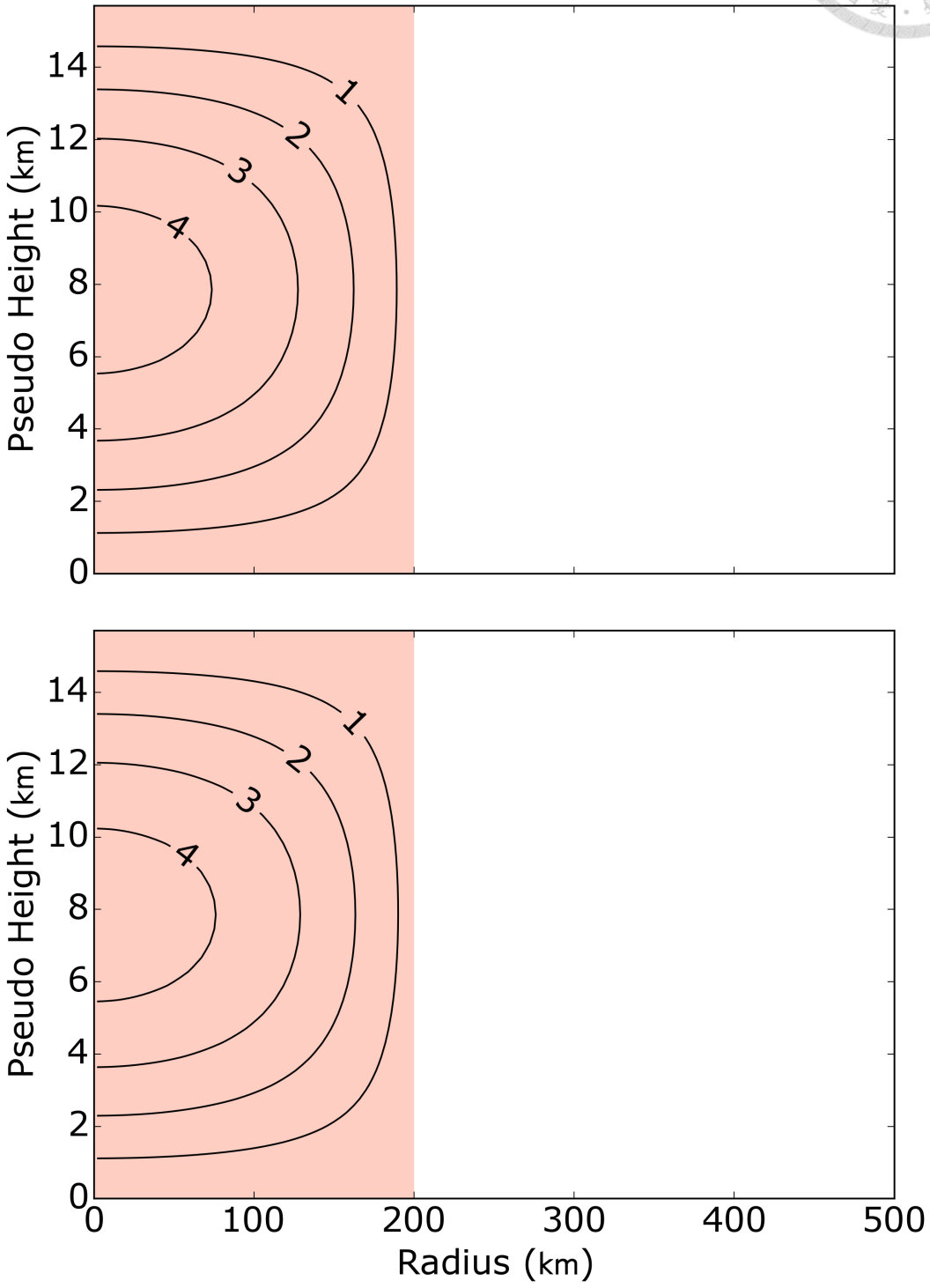

Figure 15: Distribution of dynamic efficiency of heat (%, contour) solved under barotropic (upper panel) and baroclinic (lower panel) conditions.

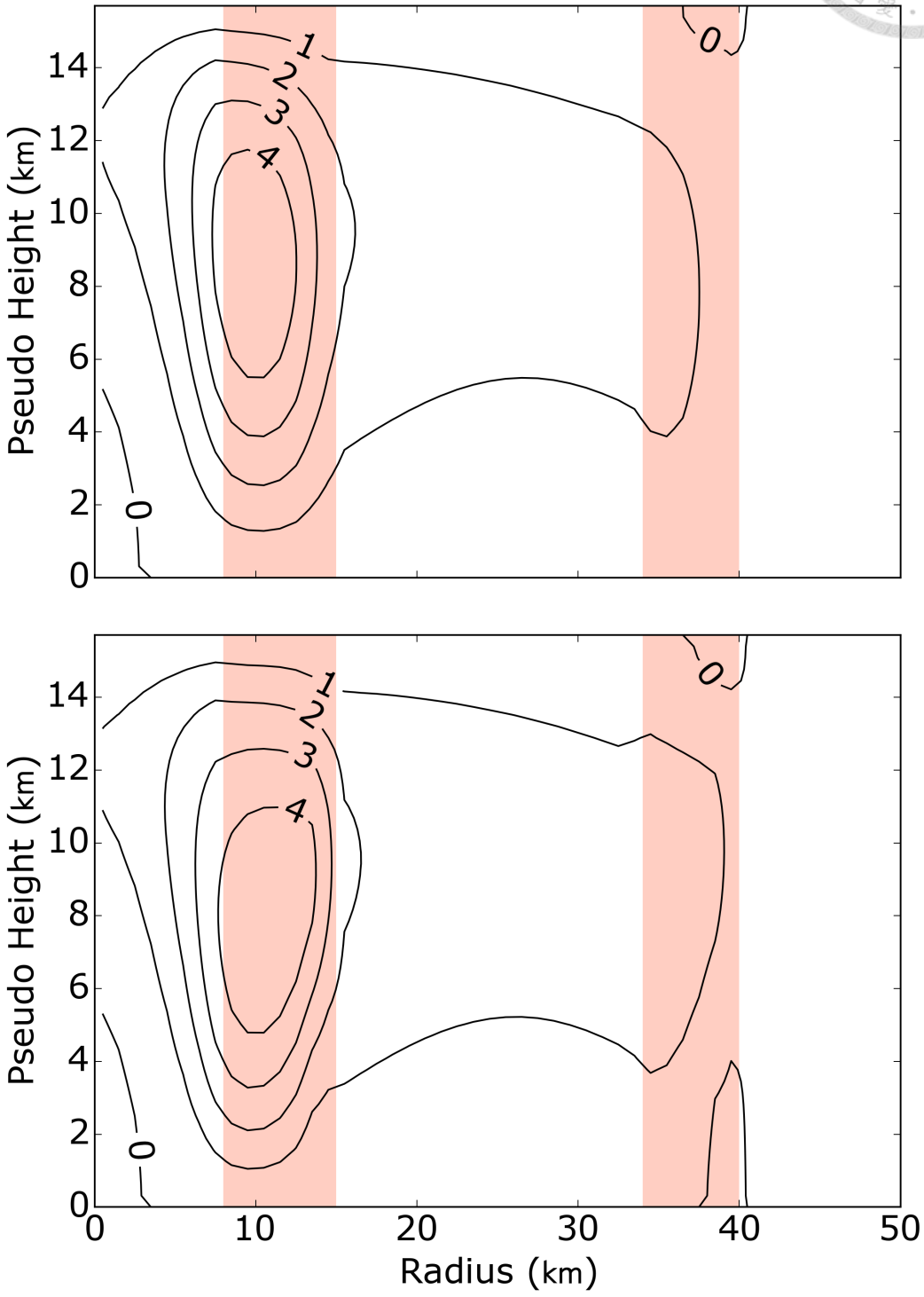

Figure 16: Distribution of dynamic efficiency of heat (%, contour) solved under barotropic (upper panel) and baroclinic (lower panel) conditions.

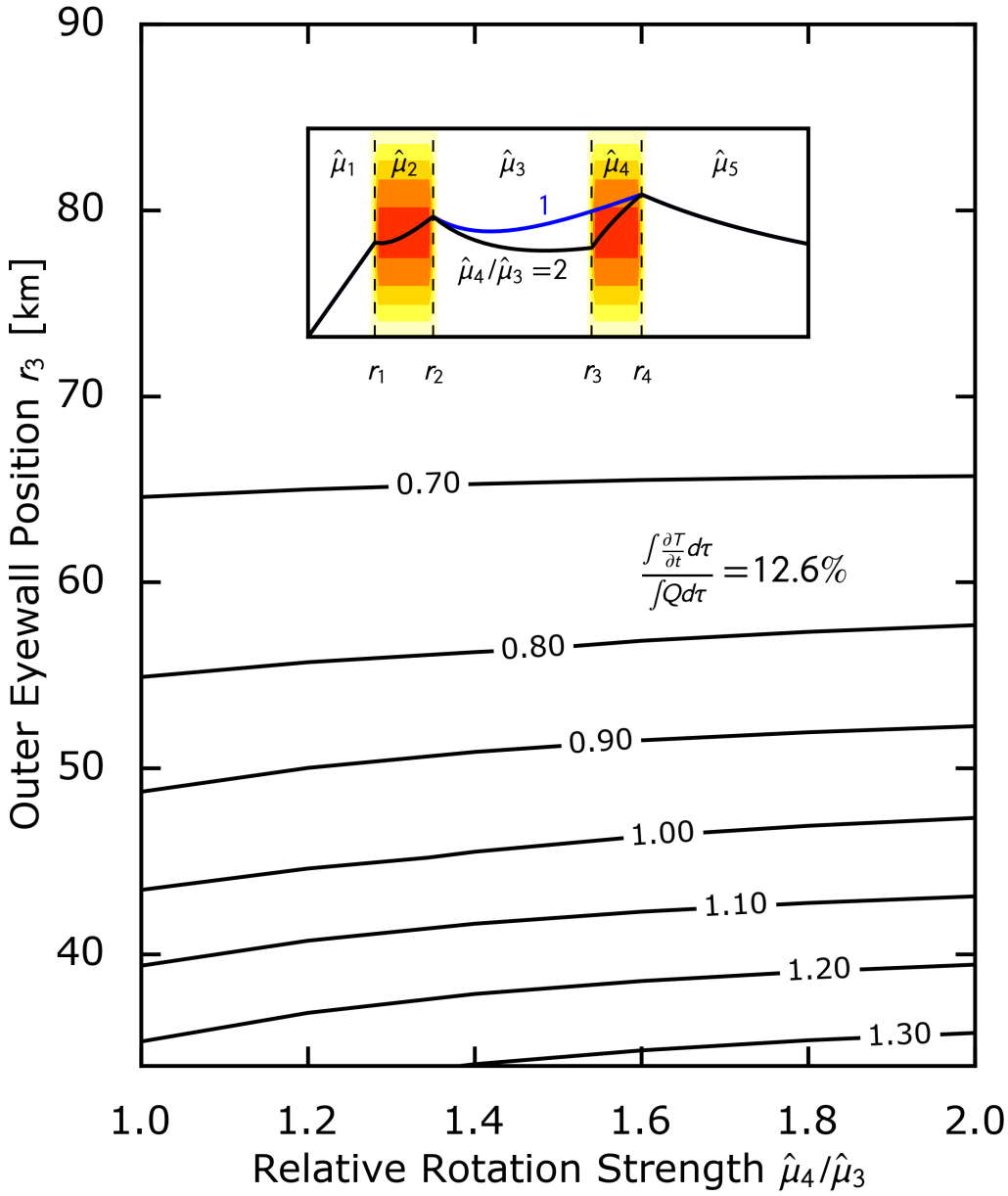

Figure 17: Average dynamic efficiency of heat $\overline{\eta}$ (%) in terms of relative rotation strength $\hat{\mu}_4/\hat{\mu}_3$ and outer eyewall position r_3 (km). Total local heat response is 12.6% throughout the domain.

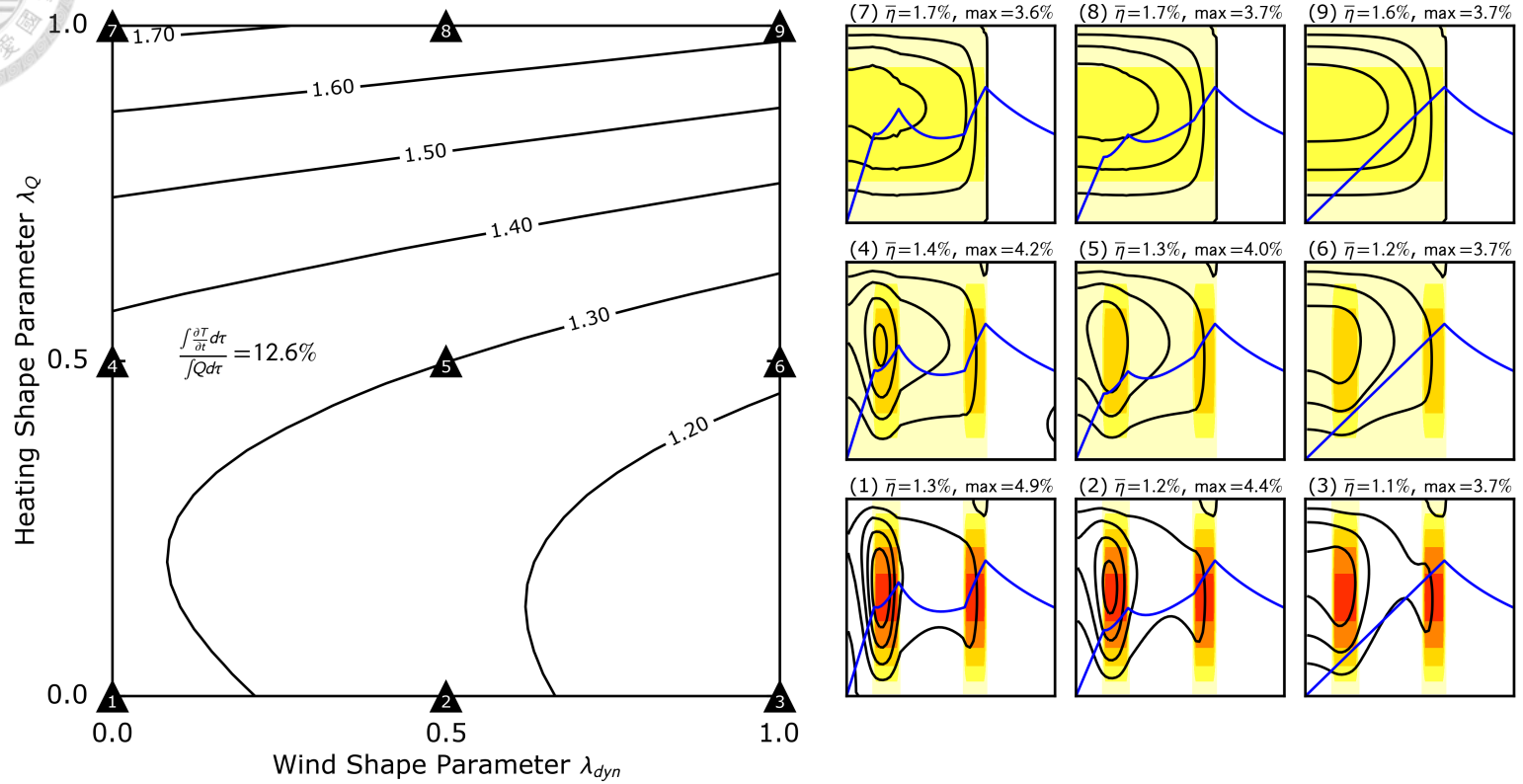

Figure 18: Average dynamic efficiency of heat $\overline{\eta}$ (%) in terms of wind shape parameter λ_{dyn} and heating shape parameter λ_Q. Nine thumbnails are drawn in the right. Total local heat response is 12.6% throughout the domain.

4.6 Internal structure of moat and outer eyewall

We conclude that the structure of heating in concentric cyclone matters. But does the structure of inertial stability matters? To alter the structure, we fix the total circulation at particular distance which equivalently implies that tangential wind speed v is fixed

$$[\text{Total circulation inside } r = r^*] = 2\pi r^* v\left(r^*\right) = \text{constant} \tag{4.11}$$

$$\Rightarrow m\left(r^*\right) = \text{constant} \tag{4.12}$$

Notice that the definition of inertial stability in 2.62, we get

$$\int_{r=0}^{r=r^*} \rho C r^3 \, dr = m^2\left(r^*\right) = \text{constant} \tag{4.13}$$

In this experiment, we use the profile C in fig. 9 and define

$$\lambda = \frac{\hat{\mu}_4}{\hat{\mu}_3} \tag{4.14}$$

to characterize the relative rotation strength between outer eyewall and moat. We analyze $1 \leq \lambda \leq 2$ and fix v at $r^* = 500$km. Moreover, we also let the size of moat vary. The result is shown Fig. 17. It shows that the structure of inertial stability has no significant effect, but the size of moat does. The latter can be realized in the sense of Rossby deformation length which is the conclusion of previous section. According to this result, we further ask: does the efficiency actually depends on the total angular momentum inside the outer eyewall?

In fig. 18, we smear the inertial stability and heating structures of single and double eyewall by define λ_Q and λ_{dyn} such that

$$\hat{Q}_k = \hat{Q}_{k,\text{ref}}\left(1 - \lambda_Q\right) + \overline{Q}\lambda_Q \tag{4.15}$$

$$\left(\hat{\mu}^2\right)_k = \left(\hat{\mu}^2\right)_{k,\text{ref}}\left(1 - \lambda_{\text{dyn}}\right) + \overline{\mu^2}\lambda_{\text{dyn}} \tag{4.16}$$

where $1 \leq k \leq 4$, $\hat{(\cdot)}_{k,\text{ref}}$ is the reference state (profile C in fig. 9), $\overline{(\cdot)}$ is the value if being constant in $r \leq r_4$.

It shows that the average efficiency is the largest if we let inertial stability structured as double eyewall while heating is distributed like single eyewall, lowest if we let inertial stability be constant and heating be like double eyewall. Diagram shows that there are at least two situations. One is the upper half where heating structure matters much more than inertial stability structure and the lower half where inertial stability matters more than the heating structure but not as significant as the former.

The results shown above let us conclude that average efficiency is linked to total heating and total circulation if we let heating be like double eyewall but wind profile varies, otherwise heating profile dominates.

4.7 Position of maximum heating

The analysis above all use the half-sined shape heating profile in z direction, so the maximum heating position would be the center of atmosphere. Now we change our heating profile with

$$Q^*(r,z) = \begin{cases} \hat{Q}^*(r) \sin\left(\pi \frac{z-(z_C-D/2)}{D}\right) & \text{if} \quad |z-z_C| \leq \frac{D}{2} \\ 0 & \text{otherwise} \end{cases} \tag{4.17}$$

where z_C is the center of the maximum heating, $D = (z_\infty - z_0)/2$ is the thickness of heating region. Fig. 13 tests various maximum heating height in different scenarios. The result roughly shows an increase of average efficiency of heat as the position gets higher.

4.8 Pre-existing baroclinity

If there is a pre-existing baroclinity, i.e. warm-core, then there exists extra potential energy in the beginning. We want to argue that $\Gamma = \sqrt{A/C}$ controls the efficiency of releasing APE. To do this, we use the following diagnose procedure:

1. Specify Γ, A, B, $C = A/\Gamma^2$, $F = Q = 0$
2. Invert χ by $\mathbf{L}\chi = \dfrac{g}{\theta_0}\dfrac{\partial\theta}{\partial r} = -B$ with $r\chi \to 0$ on boundary.
3. Calculate efficiency η_H, and boundary conversion using χ.

Fig. 14 shows that for the same strength of baroclinity, $\Gamma = 64$ has higher efficiency and higher efficiency peak position than $\Gamma = 4$. This shows that potential energy is harder for a rotation system to release. This can be understood, since when inertial stability is higher, it becomes harder for particle to move radially meaning contraction is hard, and consequently the change in kinetic energy becomes low. One might ask why this result seems to contradict 5 (strong rotation cases correspond to higher efficiency), but we have to bear in mind that this diagnose work is different from (2) because the baroclinity is prescribed rather than being a response of heating.

4.9 Sensitivity of baroclinity on the operator

Baroclinity on the operator is also driven by our heating. But in all of our experiments, $B = 0$ in the operator $\mathbf{L}$. The is because in all the cases, baroclinity is roughly 10^{-7}s^2 while A and C's order is greater than 10^{-5}s^2 which makes the crossing term not important. Fig. 15 and Fig. 16 shows the results if we exclude/include this term in the operator. Their contours are very similar which confirm our expectation.

CHAPTER 5
SUMMARY

In this study, we derive the formula of dynamic efficiency of heat and momentum. These quantities describe the kinetic energy conversion efficiency if we place heating and external momentum source at particular position. Numerical solver is based on relaxation method and is written in Fortran 95. Each experiment contains 1001 by 51 grid points and takes about 5 to 10 minutes to complete. We also design a procedure to test the response of efficiency of heat under prescribed heating profile. We test the baroclinity on the operator **L** and find it distorts the distribution of the efficiency contour slightly. We conclude this term can be neglected and still gets similar results.

Using the profile given by Schubert and Hack (1982), we found that the response of efficiency increases as vortex develops. Further analysis (Fig. 5) shows that in the young stage vortex has little ability to accumulate potential energy and low efficiency to release potential energy into kinetic energy, whilst in the latter stages it has much ability to accumulate potential energy and high efficiency to release potential energy into kinetic energy.

We also analyze concentric eyewall cases. It is shown that not only the radial position of heating but also the existence of outer eyewall enhances efficiency with notable extent. The reason for the latter is due to the reduction of Rossby deformation length.

The experiments show the structure of a vortex matters. We analyze strong rotation core (V-shaped wind profile), relative rotation strength between moat and outer eyewall, and both structure of heating and inertial stability. We find that there are two situations in which in the first situation structure of heating dominates over structure of inertial stability, and in the second situation the structure of inertial stability dominates over structure of

heating but not as significant as the former.

Next, we alter the position of maximum heating and find that the higher the heating, the better the efficiency. This result is not very physical since in most of the observations, lower atmosphere contribute most of the heating. This result needs deeper investigation.

Pre-existing baroclinity creates higher efficiency (both in strength and vertical position) if the environment is more stratified and lower efficiency if the enveronment is more rotational. This is due to its ability to make the air contract, thus it can be realized qualitatively by Rossby deformation length. When the environment is more stratified, then the Rossby deformation length is larger and makes contraction easier and thus larger energy conversion. When the environment is more rotational, then the Rossby deformation length is lower and makes contraction harder and thus lower energy conversion. It must be noted that this experiment uses different diagnose procedure – it has no prescribed heating, so we cannot mix this result with the previous experiments which include the both the processes of “accumulating” and “releasing” potential energy.

APPENDIX A
DERIVATION OF QUASI-GEOSTROPHIC EQUATIONS

A.1 Perturbation Method

Using pseudo-height as vertical coordinate, governing equations can be written as

$$\frac{\partial \vec{V}}{\partial t} + \vec{V} \cdot \nabla \vec{V} + (f_0 + \beta y)\, \hat{k} \times \vec{V} + \nabla_h \phi = \vec{F} \tag{A.1}$$

$$\frac{\partial \phi}{\partial z} = \frac{\theta}{\theta_0} g = b \tag{A.2}$$

$$\frac{\partial u}{\partial x} + \frac{\partial v}{\partial y} + \frac{\partial \rho w}{\rho \partial z} = 0 \tag{A.3}$$

$$\frac{\partial \theta}{\partial t} + \vec{V} \cdot \nabla_h \theta + w \frac{\partial \theta}{\partial z} = Q \tag{A.4}$$

where $\vec{V}$ denote horizontal velocity and ∇_h denote horizontal gradient pseudo-height z as

$$z := \frac{c_p \theta_{\text{ref}}}{g} \left[1 - \left(\frac{p}{p_{\text{ref}}} \right)^{R/c_p} \right] \tag{A.5}$$

Use the scaling

$$t = \frac{L}{U} t^* \tag{A.6}$$

$$\vec{V} = U\vec{V}^* \tag{A.7}$$

$$(x, y) = L\,(x^*, y^*) \tag{A.8}$$

$$\phi = fUL\phi^* \tag{A.9}$$

$$\nabla_h = \frac{1}{L}\nabla_h^* \tag{A.10}$$

$$\Omega = f_0\Omega^* \tag{A.11}$$

$$\beta = \frac{f_0}{a}\,(2\Omega^* \cos\phi) = \frac{f_0}{a}\beta^* \tag{A.12}$$

$$b = Bb^* \tag{A.13}$$

$$\frac{\partial b}{\partial z} = N^2 \left(\frac{\partial b}{\partial z}\right)^* \tag{A.14}$$

$$w = Ww^* \tag{A.15}$$

$$WN^2 = U\frac{B}{L} \tag{A.16}$$

where L, U are the synoptic scale, $(\,\cdot\,)^*$ is non-dimensional and a is the radius of Earth. The governing equation can be rewritten as non-dimensional version (the asterisk is omitted for simplicity)

$$R_0\frac{\partial \vec{V}}{\partial t} + R_0\vec{V}\cdot\nabla\vec{V} + (1 + R_0 y)\,\hat{k}\times\vec{V} + \nabla_h\phi = R_0\vec{F} \tag{A.17}$$

$$\frac{\partial \phi}{\partial z} = \frac{\theta}{\theta_0}g = b \tag{A.18}$$

$$\frac{\partial u}{\partial x} + \frac{\partial v}{\partial y} + R_0\frac{\partial \rho w}{\rho \partial z} = 0 \tag{A.19}$$

$$\frac{\partial b}{\partial t} + \vec{V}\cdot\nabla_h b + w\frac{\partial b}{\partial z} = Q \tag{A.20}$$

where $R_0 := U/f_0L$. Notice that we assume $L/a \sim R_0$ to prevent complication.

If we assume all non-dimensional variables have the same magnitude, then solution clearly depends on R_0. Since R_0 is generally much smaller than 1 in our consideration,

we let R_0 being our perturbation parameter. The solution may be expanded as

$$(\cdot)(R_0) = \sum_{n=0}^{\infty} R_0^n (\cdot)_n \tag{A.21}$$

Substitute this into governing equations and group terms by order of R_0. The 0th order terms give

$$\vec{V}_0 = \hat{k} \times \nabla_h \phi_0 \tag{A.22}$$

$$\frac{\partial \phi_0}{\partial z} = b_0 \tag{A.23}$$

$$\frac{\partial b_0}{\partial t} + \vec{V}_0 \cdot \nabla_h b_0 + w_0 \frac{\partial b_0}{\partial z} = Q_0 \tag{A.24}$$

The 1st order terms give

$$\frac{\partial \vec{V}_0}{\partial t} + \vec{V}_0 \cdot \nabla_h \vec{V}_0 + \hat{k} \times \vec{V}_1 + \beta y \hat{k} \times \vec{V}_0 + \nabla_h \phi_1 = \vec{F}_1 \tag{A.25}$$

$$\frac{\partial \phi_1}{\partial z} = b_1 \tag{A.26}$$

$$\nabla_h \cdot \vec{V}_1 + \frac{\partial \rho w_0}{\rho \partial z} = 0 \tag{A.27}$$

$$\frac{\partial b_1}{\partial t} + \vec{V}_0 \cdot \nabla_h b_1 + \vec{V}_1 \cdot \nabla_h b_0 + w_0 \frac{\partial b_0}{\partial z} = Q_1 \tag{A.28}$$

The above equations form the governing equations of quasi-geostrophic thoery.

A.2 Balanced Condition

If the flow is zonally periodic and balanced in y-direction

$$\frac{\partial v_0}{\partial t} + \vec{V}_0 \cdot \nabla_h v_0 = 0 \tag{A.29}$$

then take zonal mean governing equations of 0th-order

$$(\overline{u}_0, \overline{v}_0) = \left(-\frac{\partial \overline{\phi}_0}{\partial y}, 0 \right) \tag{A.30}$$

$$\frac{\partial \overline{\phi}_0}{\partial z} = \overline{b}_0 \tag{A.31}$$

$$\frac{\partial \overline{b}_0}{\partial t} + \overline{w}_0 \frac{\partial \overline{b}_0}{\partial z} = \overline{Q}_0 - \frac{\partial \overline{v_0' b_0'}}{\partial y} \tag{A.32}$$

The 1st order terms give

$$\frac{\partial \overline{u}_0}{\partial t} - \overline{v}_1 = \overline{F}_{1,x} - \frac{\partial \overline{v_0' u_0'}}{\partial y} \tag{A.33}$$

$$\overline{u_1} + \beta y \overline{u}_0 + \frac{\partial \overline{\phi}_1}{\partial y} = \overline{F}_y \tag{A.34}$$

$$\frac{\partial \overline{\phi}_1}{\partial z} = \overline{b}_1 \tag{A.35}$$

$$\frac{\partial \overline{v}_1}{\partial y} + \frac{\partial \rho \overline{w}_0}{\rho \partial z} = 0 \tag{A.36}$$

$$\frac{\partial \overline{b}_1}{\partial t} + \overline{w}_0 \frac{\partial \overline{b}_0}{\partial z} = \overline{Q}_1 - \frac{\partial \overline{v_0' b_1'}}{\partial y} \tag{A.37}$$

Collect suitable equations from above (0th order equations, zonal momentum equation and continuity from 1st order equations) we finally get

$$\frac{\partial \overline{u}_0}{\partial t} - \overline{v}_1 = \overline{F}_{1,x} - \frac{\partial \overline{v_0' u_0'}}{\partial y} \tag{A.38}$$

$$\frac{\partial \overline{b}_0}{\partial t} + \overline{w}_0 \frac{\partial \overline{b}_0}{\partial z} = \overline{Q}_0 - \frac{\partial \overline{v_0' b_0'}}{\partial y} \tag{A.39}$$

$$\frac{\partial \overline{v}_1}{\partial y} + \frac{\partial \rho \overline{w}_0}{\rho \partial z} = 0 \tag{A.40}$$

$$\frac{\partial \overline{\phi}_0}{\partial z} = \overline{b}_0 \tag{A.41}$$

$$\overline{u}_0 = -\frac{\partial \overline{\phi}_0}{\partial y} \tag{A.42}$$

We replace u_0 by u_g, v_0 by v_g, v_1 by v_a, drop all other subscripts and recover our

dimension to get more conventional notations

$$\frac{\partial \overline{u}_g}{\partial t} - f_0 \overline{v}_a = \overline{F} - \frac{\partial \overline{v'_g u'_g}}{\partial y} = \overline{F}^* \tag{A.43}$$

$$\frac{\partial \overline{b}}{\partial t} + \overline{w}\frac{\partial \overline{b}}{\partial z} = \overline{Q} - \frac{\partial \overline{v'b'}}{\partial y} = \overline{Q}^* \tag{A.44}$$

$$\frac{\partial \overline{v}_a}{\partial y} + \frac{\partial \rho \overline{w}}{\rho \partial z} = 0 \tag{A.45}$$

$$\frac{\partial \overline{\phi}}{\partial z} = \overline{b} \tag{A.46}$$

$$\overline{u}_g = -\frac{1}{f_0}\frac{\partial \overline{\phi}}{\partial y} \tag{A.47}$$

The equation above are the governing equations given in section 2.1.

APPENDIX B

WAVES AND THE ELIASSEN-SAWYER CIRCULATION EQUATION

Eliassen circulation equation is primarily based on balanced state, in which buoyancy waves cannot exist. In this appendix we will use perturbation method to include buoyancy wave. We will also see that the frequency product of horizontal and vertical direction is a constant constrained by Jacobian of angular momentum and buoyancy.

Consider the following primitive equations in Cartesian space which is symmetric in x-direction and its vertical coordinate z is physical height

$$\frac{\partial u}{\partial t} + v\frac{\partial u}{\partial y} + w\frac{\partial u}{\partial z} = fv + F, \tag{B.1a}$$

$$\frac{\partial v}{\partial t} + v\frac{\partial v}{\partial y} + w\frac{\partial v}{\partial z} = -fu - \frac{1}{\rho}\frac{\partial p}{\partial y}, \tag{B.1b}$$

$$\frac{\partial w}{\partial t} + v\frac{\partial w}{\partial y} + w\frac{\partial w}{\partial z} = -g - \frac{1}{\rho}\frac{\partial p}{\partial z}, \tag{B.1c}$$

$$\frac{\partial v}{\partial y} + \frac{\partial w}{\partial z} = 0, \tag{B.1d}$$

$$\frac{\partial \theta}{\partial t} + v\frac{\partial \theta}{\partial y} + w\frac{\partial \theta}{\partial z} = Q, \tag{B.1e}$$

in which sound waves are eliminated by letting $\mathrm{d}\rho/\mathrm{d}t = 0$.

We define "geostrophic state" as the state when

$$\frac{\overline{\mathrm{d}}}{\mathrm{d}t}\overline{(\,\cdot\,)} = 0, \tag{B.2}$$

where

$$\frac{\overline{\mathrm{d}}}{\mathrm{d}t} = \frac{\partial}{\partial t} + \overline{v}\frac{\partial}{\partial y} + \overline{w}\frac{\partial}{\partial z}. \tag{B.3}$$

for all variables and $Q = F = 0$. From (B.1a)-(B.1c) we have

$$\overline{v} = 0, \tag{B.4a}$$

$$\overline{u} = -\frac{1}{f\overline{\rho}}\frac{\partial \overline{p}}{\partial y}, \tag{B.4b}$$

$$\frac{\partial \overline{p}}{\partial z} = -\overline{\rho}g, \tag{B.4c}$$

$$\frac{\partial \overline{w}}{\partial z} = 0. \tag{B.4d}$$

Since t does not appear explicitly in (B.4a)-(B.4d), we set

$$\frac{\partial}{\partial t}\overline{(\,\cdot\,)} = 0. \tag{B.5}$$

Thermal wind relation can be derived through (B.4b) and (B.4c) as

$$f\left(\frac{1}{\overline{\rho}}\frac{\partial \overline{\rho}}{\partial z} + \frac{\partial \overline{u}}{\partial z}\right) = g\left(\frac{1}{\gamma \overline{p}}\frac{\partial \overline{p}}{\partial y} - \frac{1}{\overline{\theta}}\frac{\partial \overline{\theta}}{\partial y}\right), \tag{B.6}$$

where $\gamma = c_p/c_v$. If we assume variation of $\overline{p}$ in y and variation of $\overline{\rho}$ in z are at least an order less than others, then we obtain

$$f\frac{\partial \overline{u}}{\partial z} \approx -\frac{g}{\overline{\theta}}\frac{\partial \overline{\theta}}{\partial y}. \tag{B.7}$$

Integrating (B.4d) with z, we obtain

$$\overline{w} = \text{constant} = 0. \tag{B.8}$$

otherwise $\overline{w} \neq 0$ on top and bottom boundaries.

Letting all variables be perturbed by a small amplitude, i.e. $(\,\cdot\,) = \overline{(\,\cdot\,)} + (\,\cdot\,)'$, and

retaining the first order of (B.1a)-(B.1e) , we obtain

$$\frac{\partial \overline{\rho} u'}{\partial t} + \overline{\rho} v' \left(\frac{\partial \overline{u}}{\partial y} - f \right) + \overline{\rho} w' \frac{\partial \overline{u}}{\partial z} = \overline{\rho} F, \tag{B.9a}$$

$$\frac{\partial \overline{\rho} v'}{\partial t} = -f \overline{\rho} u' - \frac{\partial p'}{\partial y}, \tag{B.9b}$$

$$\frac{\partial \overline{\rho} w'}{\partial t} = -\frac{\partial p'}{\partial z} + \overline{\rho} \left(\frac{\theta'}{\overline{\theta}} g \right), \tag{B.9c}$$

$$\frac{\partial \overline{\rho} v'}{\partial y} + \frac{\partial \overline{\rho} w'}{\partial z} = 0, \tag{B.9d}$$

$$\frac{\partial}{\partial t} \left(\frac{\theta'}{\overline{\theta}} g \right) + \overline{\rho} v' \frac{g}{\overline{\theta}} \frac{\partial \overline{\theta}}{\partial y} + w' \frac{g}{\overline{\theta}} \frac{\partial \overline{\theta}}{\partial z} = \frac{g}{\overline{\theta}} Q, \tag{B.9e}$$

in which we approximate

$$\frac{\rho'}{\overline{\rho}} \approx -\frac{\theta'}{\overline{\theta}}. \tag{B.10}$$

under the physical sense that sound wave is relatively fast in our scale. Equation (B.9d) enables us to write

$$(\overline{\rho} v', \overline{\rho} w') = \left(-\frac{\partial \psi}{\partial z}, \frac{\partial \psi}{\partial y} \right). \tag{B.11a}$$

After taking z and y derivative of (B.9b) and (B.9c), respectively, we derive an modified version of thermal wind relation

$$f \frac{\partial \overline{\rho} u'}{\partial z} + \frac{\partial}{\partial y} \left(\overline{\rho} g \frac{\theta'}{\overline{\theta}} \right) = \frac{\partial}{\partial t} \left(\frac{\partial \overline{\rho} w'}{\partial y} - \frac{\partial \overline{\rho} v'}{\partial z} \right) = \frac{\partial}{\partial t} \left(\frac{\partial^2}{\partial y^2} + \frac{\partial^2}{\partial z^2} \right) \psi. \tag{B.12}$$

We define

$$\text{Static stability:} \quad A = \frac{g}{\overline{\theta}} \frac{\partial \overline{\theta}}{\partial z}, \tag{B.13a}$$

$$\text{Baroclinity:} \quad B = f \frac{\partial \overline{u}}{\partial z} = -\frac{g}{\overline{\theta}} \frac{\partial \overline{\theta}}{\partial y}, \tag{B.13b}$$

$$\text{Inertial stability:} \quad C = f \left(f - \frac{\partial \overline{u}}{\partial y} \right). \tag{B.13c}$$

to rewrite (B.9a) and (B.9e) as

$$f\frac{\partial\overline{\rho}u'}{\partial t} - \overline{\rho}v'C + \overline{\rho}w'B = fF, \tag{B.14a}$$

$$\frac{\partial}{\partial t}\left(\overline{\rho}g\frac{\theta'}{\overline{\theta}}\right) - \overline{\rho}v'B + \overline{\rho}w'A = \frac{g}{\overline{\theta}}Q. \tag{B.14b}$$

Adding ∂(B.14a)$/\partial z$ and ∂(B.14b)$/\partial y$, substituting (B.11a) and (B.12) into it, we get

$$\frac{\partial^2}{\partial t^2}\left(\frac{\partial^2}{\partial y^2}+\frac{\partial^2}{\partial z^2}\right)\psi + \mathbf{L}\psi = \frac{\partial}{\partial y}\left(\frac{gQ}{\overline{\theta}}\right) + f\frac{\partial F}{\partial z}, \tag{B.15a}$$

where

$$\mathbf{L}\left(\,\cdot\,\right) = \frac{\partial}{\partial y}\left(A\frac{\partial\left(\,\cdot\,\right)}{\partial y} + B\frac{\partial\left(\,\cdot\,\right)}{\partial z}\right) + \frac{\partial}{\partial z}\left(B\frac{\partial\left(\,\cdot\,\right)}{\partial y} + C\frac{\partial\left(\,\cdot\,\right)}{\partial z}\right), \tag{B.15b}$$

which is elliptic if $B^2 - AC < 0$.

Neglecting Q, F and assuming A, C are constants, dispersion relation given by (B.15a) is

$$\omega^2\left(l^2+m^2\right) = Al^2 + 2Blm + Cm^2, \tag{B.16}$$

where ω, l and m are wavenumber of t, y and z. (B.16) reduces to purely dispersion relation in usual buoyancy wave system if there is no baroclinity, i.e. $B = 0$,

$$\omega^2\left(l^2+m^2\right) = Al^2 + Cm^2. \tag{B.17}$$

Let

$$\sin\theta = \frac{l}{\kappa}, \tag{B.18a}$$

$$\cos\theta = \frac{m}{\kappa}, \tag{B.18b}$$

where $\kappa = \sqrt{l^2 + m^2}$. Substituting (B.18b)-(B.18a) into (B.16), we get

$$\begin{aligned}
\omega^2 &= A\sin^2\theta + B\sin\theta\,\cos\theta + C\cos^2\theta \\
&= \frac{A}{2}(1-\cos 2\theta) + B\sin 2\theta + \frac{C}{2}(1+\cos 2\theta) \\
&= \frac{C+A}{2} + \frac{C-A}{2}\cos 2\theta + B\sin 2\theta \\
&= \frac{C+A}{2} + \sqrt{B^2 + \left(\frac{C-A}{2}\right)^2}\sin(2\theta+\alpha),
\end{aligned} \tag{B.19}$$

where α is designed as

$$\sin\alpha = \frac{(C-A)/2}{\sqrt{B^2 + \left(\frac{C-A}{2}\right)^2}}, \tag{B.20a}$$

$$\cos\alpha = \frac{B}{\sqrt{B^2 + \left(\frac{C-A}{2}\right)^2}}, \tag{B.20b}$$

to apply sum-to-product identities.

To get the group velocity, we first notice

$$\begin{aligned}
\nabla &= \left(\frac{\partial}{\partial l}, \frac{\partial}{\partial m}\right) \\
&= \left(\frac{\partial\cos\theta}{\partial l}\frac{\mathrm{d}\theta}{\mathrm{d}\cos\theta}\frac{\mathrm{d}}{\mathrm{d}\theta}, \frac{\partial\sin\theta}{\partial l}\frac{\mathrm{d}\theta}{\mathrm{d}\sin\theta}\frac{\mathrm{d}}{\mathrm{d}\theta}\right) \\
&= (m, -l)\,\frac{1}{\kappa^2}\frac{\mathrm{d}}{\mathrm{d}\theta}.
\end{aligned} \tag{B.21}$$

Applying (B.21) to (B.16), we get

$$\begin{aligned}
(c_{gx}, c_{gy}) &= \nabla\omega \\
&= \frac{1}{\omega\kappa^2}\sqrt{B^2 + \left(\frac{C-A}{2}\right)^2}\cos(2\theta+\alpha)\,(m,-l).
\end{aligned} \tag{B.22}$$

So the direction of energy transport is orthogonal to the wave geometry whose amplitude is controlled by A, B, and C.

Possible range of ω^2 is

$$\left| \omega^2 - \frac{C+A}{2} \right| \leq \sqrt{B^2 + \left(\frac{C-A}{2} \right)^2}. \tag{B.23}$$

The stable solution requires $\omega^2 > 0$,

$$\frac{C+A}{2} - \sqrt{B^2 + \left(\frac{C-A}{2} \right)^2} > 0 \tag{B.24}$$

$$\Rightarrow \; B^2 - AC < 0, \tag{B.25}$$

which is equivalent to require the time-independent part of (B.15a) to be elliptic. The maximum and minimum frequencies are

$$\omega_{\text{max}} = \frac{C+A}{2} + \sqrt{B^2 + \left(\frac{C-A}{2} \right)^2}, \tag{B.26a}$$

$$\omega_{\text{min}} = \frac{C+A}{2} - \sqrt{B^2 + \left(\frac{C-A}{2} \right)^2}, \tag{B.26b}$$

and their product is

$$\omega_{\text{max}} \, \omega_{\text{min}} = AC - B^2. \tag{B.27}$$

(B.27) implies the stiffnes of the system is controlled by $AC - B^2$ variable only. If on direction gets stiffer, it will be accompanied by the relaxation of the other direction.

The quantity $AC - B^2$ is actually the Jacobian of absolute angular momentum and buoyancy force

$$\overline{m} = f\left(fy - \overline{u}\right), \tag{B.28a}$$

$$\overline{b} = g \ln\left(\frac{\overline{\theta}}{\theta_0} \right), \tag{B.28b}$$

which is shown as follows

$$\begin{aligned} AC - B^2 &= \frac{g}{\overline{\theta}} \frac{\partial \overline{\theta}}{\partial z} f \left(f - \frac{\partial \overline{u}}{\partial y} \right) + f \frac{\partial \overline{u}}{\partial z} \frac{g}{\overline{\theta}} \frac{\partial \overline{\theta}}{\partial y} \\ &= \frac{\partial \overline{b}}{\partial z} \frac{\partial \overline{m}}{\partial y} - \frac{\partial \overline{m}}{\partial z} \frac{\partial \overline{b}}{\partial y} \\ &= \frac{\partial \left(\overline{m}, \overline{b} \right)}{\partial \left(y, z \right)}. \end{aligned} \tag{B.29}$$

The condition (B.15b) is elliptic if $B^2 - AC$ can be realized through the example shown in Fig. 19, 20, and through the use of B.29. m controls the movement in y direction, when an air parcel is displaced from its original position, it will oscillate back to its original y position. The same is also true for b, but in z direction. The composite effect gives Fig. 19 a stable configuration in which the displaced air parcel tends to go back its original position, corresponding to (B.29) being positive (elliptic), and Fig. 20 an unstable configuration in which the displaced air parcel tends to move away from its original position, corresponding to (B.29) being negative (non-elliptic).

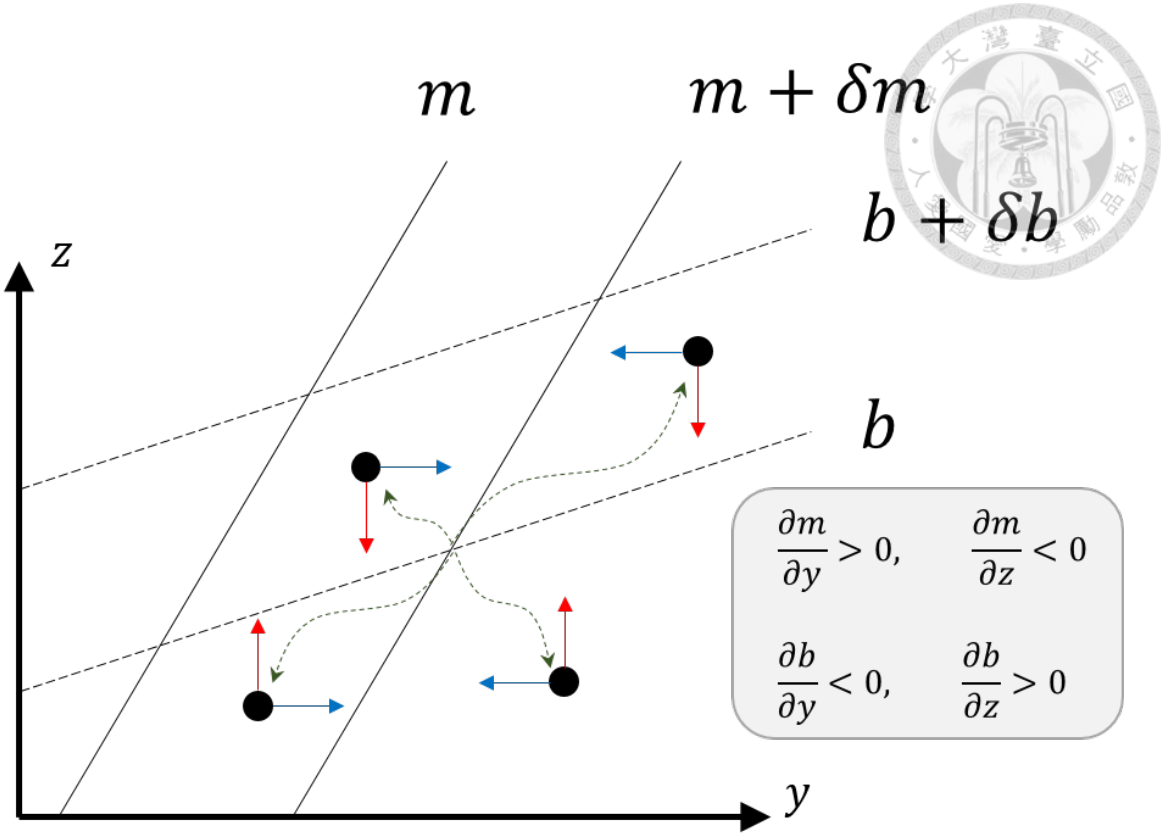

Figure 19: A stable configuration of m and b. The red and blue arrows are buoyancy restorcing force and inertial restoring force, respectively.

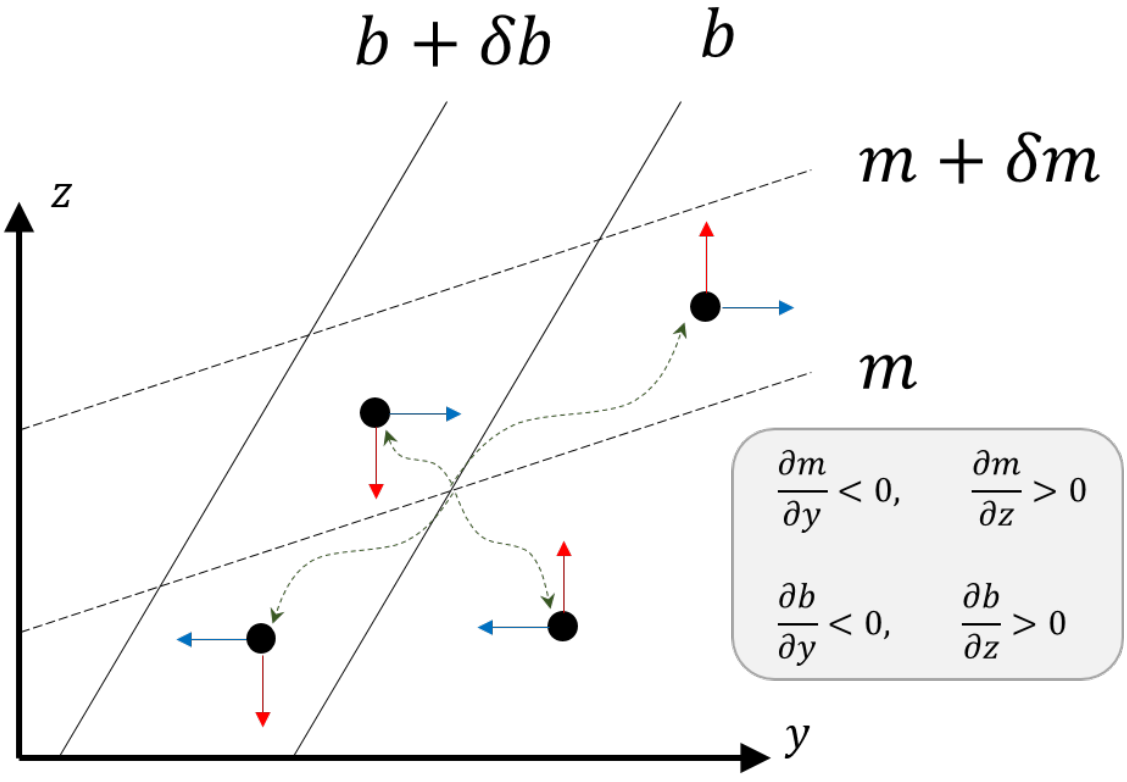

Figure 20: An unstable configuration of m and b. The red and blue arrows are buoyancy restorcing force and inertial restoring force, respectively.

APPENDIX C
BOUNDARY CONVERSION

In the derivation of efficiency, we apply boundary condition for $r\psi$ and $r\chi$ to get the desired self-adjoint property (equation [2.71]). However when dealing with open boundary condition, i.e. when Ekman pumping is considered, extra terms appear.

If we restrict ourselves by considering bottom-opened scenario (which is reasonable since in a tropical cyclone dynamical influence usually comes from bottom), we will require $r\psi \to 0$ as $r \to 0, \infty$ or as $z \to z_\infty$. Apply integral by parts to LHS of equation (2.71)

$$\iint \psi \mathbf{L}\chi \; r\mathrm{d}r\mathrm{d}z = \iint \chi \mathbf{L}\psi \; r\mathrm{d}r\mathrm{d}z + \int \left(C\psi \frac{\partial \chi}{\partial z} \right) \Bigg|_{z_0}^{z_\infty} r\mathrm{d}r \tag{C.1}$$

The second term due to boundary condition is called *boundary conversion*, denoted as $\mathbf{C}_B$, characterizing the effect of boundary condition on $r\psi$ (vertical motion). This term depends only on boundary condition and χ (or temperature profile $\theta\,(r, z)$) but not on diabatic heating Q nor external forcing F.

APPENDIX D

SIMILARITY BETWEEN CYLINDRICAL AND SPHERICAL COORDINATES

In this appendix we would prove that governing equations in cylindrical coordinates (Sec. 2.3) and spherical coordinates (Sec. 2.4) are essentially identical but with minor difference.

For clarity we list again the governing equations in both coordinates [(2.59) and (2.83)] and arrange them in proper order. We also redefine geopotential ϕ in cylindrical coordinates as G to avoid obfuscation.

Cylindrical coordinates:

$$\frac{\partial m}{\partial t} + u\frac{\partial m}{\partial r} + w\frac{\partial m}{\partial z} = rF, \quad \text{(D.1a)}$$

$$\frac{\partial \theta}{\partial t} + u\frac{\partial \theta}{\partial r} + w\frac{\partial \theta}{\partial z} = Q, \quad \text{(D.1b)}$$

$$\frac{\partial G}{\partial r} = \frac{1}{r^3}\left(m^2 - \frac{1}{4}f^2r^4\right), \quad \text{(D.1c)}$$

$$\frac{\partial G}{\partial z} = \frac{\theta}{\theta_0}g, \quad \text{(D.1d)}$$

$$\frac{\partial ru}{r\partial r} + \frac{\partial \rho w}{\rho \partial z} = 0. \quad \text{(D.1e)}$$

where $m = rv + 1/2fr^2$.

Spherical coordinates:

$$\frac{\partial m}{\partial t} + v\frac{\partial m}{\partial (a\phi)} + w\frac{\partial m}{\partial z} = RF, \quad \text{(D.2a)}$$

$$\frac{\partial \theta}{\partial t} + v\frac{\partial \theta}{\partial (a\phi)} + w\frac{\partial \theta}{\partial z} = Q, \quad \text{(D.2b)}$$

$$\frac{\sin\phi}{R^3}\left(m^2 - \Omega^2R^4\right) = -\frac{\partial G}{\partial (a\phi)}, \quad \text{(D.2c)}$$

$$\frac{\partial G}{\partial z} = \frac{\theta}{\theta_0}g, \quad \text{(D.2d)}$$

$$\frac{\partial Rv}{R\partial (a\phi)} + \frac{\partial \rho w}{\rho \partial z} = 0. \quad \text{(D.2e)}$$

where $m = Ru + \Omega R^2$.

After speculation and with the aid of Fig. 21, we notice that there are two types of "radius". One is the coordinate radius $\tilde{r}$ while the other is the radius $\tilde{R}\left(\tilde{r}\right)$ with respect to the rotation

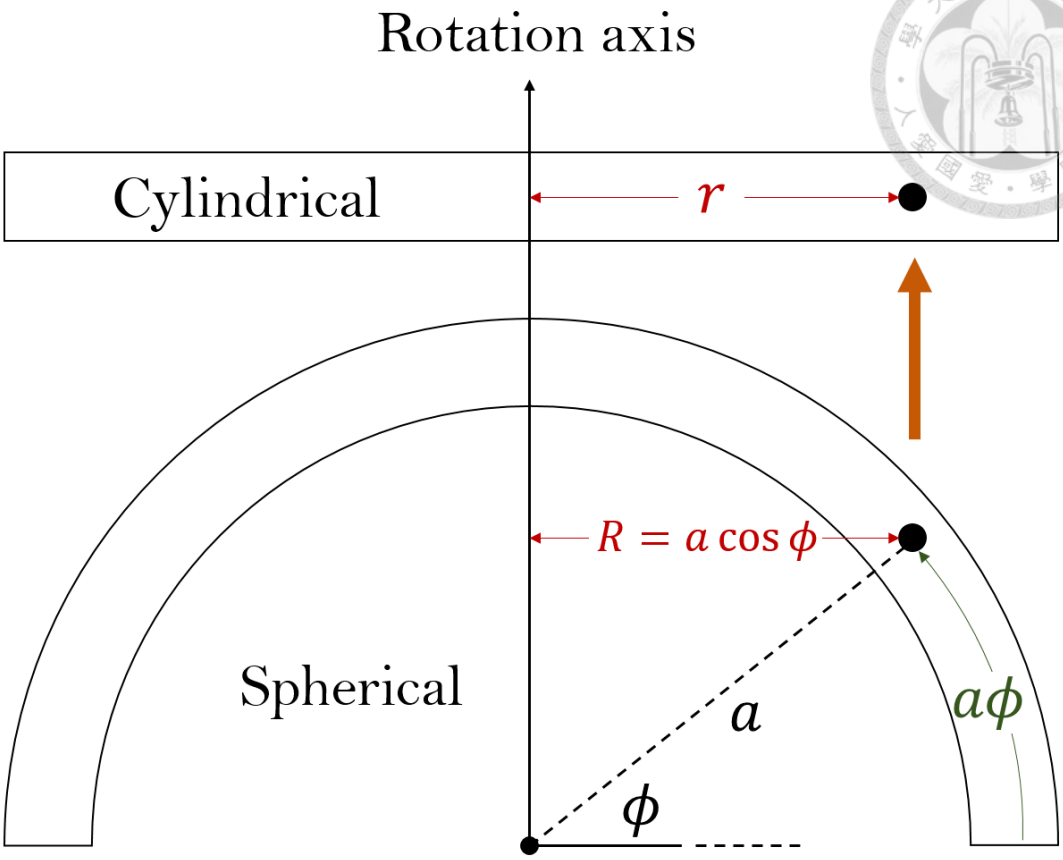

Figure 21: The comparison between cylindrical and spherical coordinates.

center. The following gives more general governing equations.

$$\text{Absolute angular momentum:} \quad \frac{\partial m}{\partial t} + \tilde{u}\frac{\partial m}{\partial \tilde{r}} + w\frac{\partial m}{\partial z} = \tilde{R}F, \tag{D.3a}$$

$$\text{Thermodynamic:} \quad \frac{\partial \theta}{\partial t} + \tilde{u}\frac{\partial \theta}{\partial \tilde{r}} + w\frac{\partial \theta}{\partial z} = Q, \tag{D.3b}$$

$$\text{Balanced condition:} \quad \frac{\tilde{S}\left(\tilde{r}\right)}{\tilde{R}^3}\left(m^2 - \tilde{\Omega}^2\tilde{R}^4\right) = \frac{\partial G}{\partial \tilde{r}}, \tag{D.3c}$$

$$\text{Hydrostatic:} \quad \frac{\partial G}{\partial z} = \frac{\theta}{\theta_0}g, \tag{D.3d}$$

$$\text{Continuity:} \quad \frac{\partial \tilde{R}\tilde{u}}{\tilde{R}\partial \tilde{r}} + \frac{\partial \rho w}{\rho \partial z} = 0. \tag{D.3e}$$

where $m = \tilde{R}\tilde{v} + \tilde{\Omega}\tilde{R}^2$ is the absolute angular momentum, $\tilde{v}$ is the main circulation, $\tilde{u} = \mathrm{d}\tilde{r}/\mathrm{d}t$ together with w represents the secondary circulation, and $\tilde{S}\left(\tilde{r}\right)$ is a parameter depending only on $\tilde{r}$.

By (D.3c) and (D.3d), we derive the thermal wind relation

$$\frac{g}{\theta_0}\frac{\partial\theta}{\partial\tilde{r}} = \frac{\tilde{S}}{\tilde{R}^3}\frac{\partial m^2}{\partial z}, \tag{D.4}$$

in which we notice that the parameter $\tilde{S}$ is a minor issue since it depends only on horizontal direction so it would not involve in the operation when deriving thermal wind relation.

After taking time derivative of (D.4), we get

$$\frac{\partial}{\partial t}\left(\frac{g}{\theta_0}\frac{\partial\theta}{\partial\tilde{r}}\right) = \frac{\partial}{\partial t}\left(\frac{\tilde{S}}{\tilde{R}^3}\frac{\partial m^2}{\partial z}\right). \tag{D.5}$$

We define

$$\text{Static stability:}\quad \rho A = \frac{g}{\theta_0}\frac{\partial\theta}{\partial z}, \tag{D.6a}$$

$$\text{Baroclinity:}\quad \rho B = -\frac{g}{\theta_0}\frac{\partial\theta}{\partial\tilde{r}} = -\frac{\tilde{S}}{\tilde{R}^3}\frac{\partial m^2}{\partial z}, \tag{D.6b}$$

$$\text{Inertial stability:}\quad \rho C = \frac{1}{\tilde{R}^3}\frac{\partial m^2}{\partial\tilde{r}}, \tag{D.6c}$$

to rewrite (D.3a) and (D.3b) as

$$\frac{1}{\tilde{R}^3}\frac{\partial m^2}{\partial t} + \rho\tilde{u}C - \rho wB = \frac{2mF}{\tilde{R}^2}, \tag{D.7a}$$

$$\frac{g}{\theta_0}\frac{\partial\theta}{\partial t} - \rho\tilde{u}B + \rho wA = \frac{g}{\theta_0}Q. \tag{D.7b}$$

According to (D.3e) we define the streamfunction ψ such that

$$(\rho\tilde{u}, \rho w) = \left(-\frac{\partial\psi}{\partial z}, \frac{\partial\tilde{R}\psi}{\tilde{R}\partial\tilde{r}}\right). \tag{D.8}$$

After subtracting ∂(D.7b)$/\partial\tilde{r}$ from ∂(D.7a)$/\partial z$ to eliminate partial derivative of time with the aid of (D.5) and substituting (D.8) into it, we obtain a generalized Eliassen-Sawyer circulation equation for both coordinates

$$\mathbf{L}\psi = \frac{g}{\theta_0}\frac{\partial Q}{\partial\tilde{r}} - \frac{1}{\tilde{R}^2}\frac{\partial 2mF}{\partial z}, \tag{D.9a}$$

where

$$\mathbf{L}\left(\,\cdot\,\right) = \frac{\partial}{\partial \tilde{r}}\left(A\frac{\partial \tilde{R}\left(\,\cdot\,\right)}{\tilde{R}\partial \tilde{r}} + B\frac{\partial\left(\,\cdot\,\right)}{\partial z}\right) + \frac{\partial}{\partial z}\left(B\frac{\partial \tilde{R}\left(\,\cdot\,\right)}{\tilde{R}\partial \tilde{r}} + C\frac{\partial\left(\,\cdot\,\right)}{\partial z}\right), \tag{D.9b}$$

and (D.9b) is elliptic if $B^2 - AC < 0$. The boundary conditions for (D.9a) are that $\psi = 0$ on top, bottom, and inner boundaries and $\psi \to 0$ as $r \to \infty$.

We close this part by deriving Eliassen operators for both coordinates. Using the variables defined in Table 6, we get the Eliassen operators for cylindrical coordinates

$$\mathbf{L}\left(\,\cdot\,\right) = \frac{\partial}{\partial r}\left(A\frac{\partial r\left(\,\cdot\,\right)}{\partial r}r + B\frac{\partial\left(\,\cdot\,\right)}{\partial z}\right) + \frac{\partial}{\partial z}\left(B\frac{\partial r\left(\,\cdot\,\right)}{r\partial r} + C\frac{\partial\left(\,\cdot\,\right)}{\partial z}\right), \tag{D.10}$$

where

$$\text{Static stability:} \quad \rho A = \frac{g}{\theta_0}\frac{\partial \theta}{\partial z}, \tag{D.11a}$$

$$\text{Baroclinity:} \quad \rho B = -\frac{g}{\theta_0}\frac{\partial \theta}{\partial r} = -\frac{1}{r^3}\frac{\partial m^2}{\partial z}, \tag{D.11b}$$

$$\text{Inertial stability:} \quad \rho C = \frac{1}{r^3}\frac{\partial m^2}{\partial r}, \tag{D.11c}$$

and spherical coordinates

$$\mathbf{L}\left(\,\cdot\,\right) = \frac{\partial}{\partial (a\phi)}\left(A\frac{\partial R\left(\,\cdot\,\right)}{R\partial (a\phi)} + B\frac{\partial\left(\,\cdot\,\right)}{\partial z}\right) + \frac{\partial}{\partial z}\left(B\frac{\partial R\left(\,\cdot\,\right)}{R\partial (a\phi)} + C\frac{\partial\left(\,\cdot\,\right)}{\partial z}\right), \tag{D.12}$$

where

$$\text{Static stability:} \quad \rho A = \frac{g}{\theta_0}\frac{\partial \theta}{\partial z}, \tag{D.13a}$$

$$\text{Baroclinity:} \quad \rho B = -\frac{g}{\theta_0}\frac{\partial \theta}{\partial (a\phi)} = \frac{\sin\phi}{R^3}\frac{\partial m^2}{\partial z}, \tag{D.13b}$$

$$\text{Inertial stability:} \quad \rho C = -\frac{\sin\phi}{R^3}\frac{\partial m^2}{\partial (a\phi)}. \tag{D.13c}$$

Table 6: General form of Eliassen-Sawyer circulation equation in cylindrical and spherical coordinates

Variables in (D.9b)	Cylindrical	Spherical
$\tilde{r}$	r	$a\phi$
$\tilde{R}$	r	R
$\tilde{\Omega}$	$f/2$	Ω
$\tilde{v}$	v	u
$\tilde{u}$	u	v
$\tilde{S}$	1	$-\sin\phi$

APPENDIX E

APPLICATION PROGRAMMING INTERFACE

Here we list the core API to solve (3.1). The code is written in Fortran 95 and maintained on Github (`http://github.com/meteorologytoday/XLab-EE-fortran`).

Basic usage is as follows

```
! This is a simple example of solving Eliassen-Sawyer
! circulation equation. All other variables are set
! initially with the correct type specified by API below


! #1: Calculate coefficient matrix first
err_flg = 0
call cal_coe(a, b, c, coe, dx, dy, nx, ny, err_flg)
if (err_flg /= 0) then ! Error occurs.
  exit
end if

! #2: Solve the equation
err_flg = 0
strategy = 0
strategy_r = 1e-3
call solve_elliptic(max_iter, strategy_r, 1.0, dat, coe, f, &
&                   workspace, nx, ny, err_flg, debug)
if (err_flg /= 0) then ! Error occurs
  exit
end if
```

#Subroutine:

cal_coe (a, b, c, coe, dx, dy, nx, ny, err)

#Description:

Calculate (3.8a) and store result in **coe**.

#Parameters:

– *Real(4)* :: **a (nx-1, ny-2)**

Static stability A in (3.1) whose dimension is (**nx**-1, **ny**-2).

– *Real(4)* :: **b (nx-1, ny-1)**

Static stability B in (3.1) whose dimension is (**nx**-1, **ny**-1).

– *Real(4)* :: **c (nx-2, ny-1)**

Static stability C in (3.1) whose dimension is (**nx**-2, **ny**-1).

– *Real(4)* :: **coe (9, nx, ny)**

Coefficient matrix which stores the result of this subroutine. Its dimension is (9, **nx**, **y**).

– *Real(4)* :: **dx**

Grid spacing in x direction.

– *Real(4)* :: **dy**

Grid spacing in y direction.

– *Integer* :: **nx**

Number of grid points in x direction.

– *Integer* :: **ny**

Number of grid points in y direction.

– *Integer* :: **err**

Error flag. Modified to 0 if completed and without error, otherwise not 0.

#Subroutine:

do_elliptic (psi, coe, outdat, nx, ny, err)

#Description:

Calculate **L**ψ in (3.1). Result is stored in **outdat**.

#Parameters:

– *Real(4)* :: **psi (nx, ny)**

ψ field whose dimension is (**nx**-1, **ny**-2).

– *Real(4)* :: **coe (9, nx, ny)**

Coefficient matrix calculated beforehand by Subroutine **cal_coe**.

– *Real(4)* :: **outdat (nx, ny)**

Result of $\mathbf{L}\psi$ in (3.1).

– *Integer* :: **nx**

Number of grid points in x direction.

– *Integer* :: **ny**

Number of grid points in y direction.

– *Integer* :: **err**

Error flag. Modified to 0 if completed and without error, otherwise not 0.

#Subroutine:

solve_elliptic(max_iter, strategy, strategy_r, alpha, dat, coe, f, workspace, nx, ny, err, debug)

#Description:

Invert ψ in (3.1). Boundary conditions are given in the boundaries of **f**. Result is stored in **dat**. This subroutine now provides two ways to judge the convergence which can be specified with **strategy**.

"1" specifies to judge "absolute" residue defined in (3.10) and this critical value should be given in **strategy_r**.

"2" specifies to judge "relative" variation of residue defined in (3.10) and this critical value should be given in **strategy_r**.

#Parameters:

– *Integer* :: **max_iter**

Maximum iteration time. If iteration time is reached and convergence criteria is not met, then **err** $\neq 0$.

– *Integer* :: **strategy**

Strategy used to judge convergence. See *#Description* part.

– *Real(4)* :: **strategy_r**

This value service different criteria according to **strategy**. See #*Description* part.

– *Real(4)* :: **alpha**

Over-relaxation parameter. It is recommended to set this value 1.0.

– *Real(4)* :: **dat (nx, ny)**

Result of relaxation. The initial guess of iteration can be placed in this array. Its dimension is (**nx**, **ny**).

– *Real(4)* :: **coe (9, nx, ny)**

Coefficient matrix calculated beforehand by Subroutine **cal_coe**.

– *Real(4)* :: **f (nx, ny)**

This is F in (3.1) whose dimension is (**nx**, **ny**). Notice that boundary conditions are given in the boundaries of **f**.

– *Real(4)* :: **workspace (nx, ny)**

The workspace when doing relaxation whose dimension is (**nx**, **ny**).

– *Integer* :: **nx**

Number of grid points in x direction.

– *Integer* :: **ny**

Number of grid points in y direction.

– *Integer* :: **err**

Error flag. Modified to 0 if completed and without error, otherwise not 0.

– *Integer* :: **debug**

Debug message output if 1. No debug message if 0.

BIBLIOGRAPHY

Charney, J. G., and A. Eliassen, 1964: On the growth of the hurricane depression. *J. Atmos. Sci.*, **21**, 68–75.

Hack, J. J., and W. H. Schubert, 1986: Nonlinear response of atmospheric vortices to heating by organized cumulus convection. *J. Atmos. Sci.*, **43**, 1559–1573.

Hack, J. J., W. H. Schubert, D. E. Stevens, and H.-C. Kuo, 1989: Response of the hadley circulation to convective forcing in the itcz. *J. Atmos. Sci.*, **46**, 2957–2973.

Holliday, C. R., and A. H. Thompson, 1979: Climatological characteristics of rapidly intensifying typhoons. *J. Atmos. Sci.*, **107**, 1022–1034.

Hoskins, B. J., and F. P. Bretherton, 1972: Atmospheric frontogenesis models: Mathematical formulation and solution. *J. Atmos. Sci.*, **29**, 11–37.

Hoskins, B. J., and N. V. West, 1979: Baroclinic waves and frontogenesis. part ii: Uniform potential vorticity jet flows-cold and warm fronts. *J. Atmos. Sci.*, **36**, 1663–1680.

Kuo, H.-C., C.-P. Chang, Y.-T. Yang, and J. H.-J., 2009: Western north pacific typhoons with concentric eyewalls. *Monthly Weather Review*, **137**, 3758–3770.

Rozoff, C. M., W. H. S. Schubert, and J. P. Kossin, 2008: Some dynamical aspects of tropical cyclone concentric eyewalls. *Quart. J. Roy. Meteor. Soc.*, **134**, 583–593.

Schubert, W. H., P. E. Ciesielski, C. Lu, and R. H. Johnson, 1989: Dynamical adjustment of the trade wind inversion layer. *J. Atmos. Sci.*, **52**, 2941–2952.

Schubert, W. H., and J. J. Hack, 1982: Inertial stability and tropical cyclone development. *J. Atmos. Sci.*, **39**, 1687–1697.

Schubert, W. H., and B. D. McNoldy, 2010: Application of the concepts of rossby length and rossby depth to tropical cyclone dynamics. *J. Adv. Model. Earth Syst.*, **2**, 13pp., doi:10.3894/JAMES.2010.2.7.

Schubert, W. H., C. M. Rozoff, J. L. Vigh, B. D. McNoldy, and J. P. Kossin, 2007: On the distribution of subsidence in the hurricane eye. *Quart. J. Roy. Meteor. Soc.*, **133**, 595–605.

Shea, D. J., and W. M. Gray, 1973: The hurricane's inner core retion, i: Symmetric and asymmetric structure. *J. Atmos. Sci.*, **30**, 1544–1564.

Simpson, R. H., and L. G. Starrett, 1955: Further studies of hurricane structure by aircraft reconnaissance. *Bull. Am. Meteorol. Soc.*, **36**, 459–468.

Yang, Y.-T., E. A. Kuo, H.-C. Hendricks, and M. S. Peng, 2013: Structural and intensity changes of concentric eyewall typhoons in the western north pacific basin. *Monthly Weather Review*, **141**, 2632–2648.